10(2013) 349 – 390

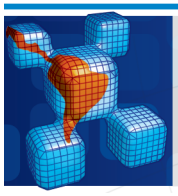

Latin American Journal of Solids and Structures
www.lajss.org

Dynamic Analysis and Critical Speed of Rotating Laminated Conical Shells with Orthogonal Stiffeners Using Generalized Differential Quadrature Method

Abstract

This paper presents effects of boundary conditions and axial loading on frequency characteristics of rotating laminated conical shells with meridional and circumferential stiffeners, i.e., stringers and rings, using Generalized Differential Quadrature Method (GDQM). Hamilton's principle is applied when the stiffeners are treated as discrete elements. The conical shells are stiffened at uniform intervals and it is assumed that the stiffeners have similar material and geometric properties. Equations of motion as well as equations of the boundary condition are transformed into a set of algebraic equations by applying the GDQM. Obtained results discuss the effects of parameters such as rotating velocities, depth to width ratios of the stiffeners, number of stiffeners, cone angles, and boundary conditions on natural frequency of the shell. The results will then be compared with those of other published works particularly with a non-stiffened conical shell and a special case where angle of the stiffened conical shell approaches zero, i.e. a stiffened cylindrical shell. In addition, another comparison is made with present FE method for a non-rotating stiffened conical shell. These comparisons confirm reliability of the present work as a measure to approximate solutions to the problem of rotating stiffened conical shells.

Keywords

Rotating laminated conical shells, Stringer/ring stiffener, Natural Frequency, Generalized Differential Quadrature Method (GDQM), Critical Speed.

Kamran Daneshjou [1], **Mostafa Talebitooti** [2, *], **Roohollah Talebitooti** [3], **Hamed Saeidi Googarchin** [4]

1 Prof., Sch. of Mech. Eng., Iran University of Science and Technology, Tehran, Iran
2 Ph.D. Stu., Sch. of Mech. Eng., Iran University of Science and Technology, Tehran, Iran
3 Assist. Prof., Sch. of Auto. Eng., Iran University of Science and Technology, Tehran, Iran
4 Ph.D. Stu., Sch. of Mech. Eng. , K.N.T University of Technology, Tehran, Iran

Received 04 Mar 2012
In revised form 12 Jun 2012

* Author email: mtalebi@iust.ac.ir

1 INTRODUCTION

Circular and conical shell structures are widely being used in many branches of engineering. Vibration of these structures has been also extensively studied [1-3]. Meanwhile, rotating cylindrical and conical shells were studied by many researchers.

Nomenclature

A_{ij}	extensional stiffness	$N_{s(or\ r)}$	number of stringers (or rings)
$A_{s(or\ r)}$	cross sectional area of stringers (or rings)	Q_{ij}	reduced stiffness matrix
A^*	defined by Eq. (51)	$\bar{Q}_{ij}$	transformed reduced stiffness matrix
a	minor radius of conical shell	R	defined by Eq. (39)
B_{ij}	coupling stiffness	r_x	radius at any coordinate point x , ϑ, z
B^*	defined by Eq. (51)	$\mathbf{r}$	displacement vector
b	major radius of conical shell	S_{ij}	stiffness matrix
$b_{s(or\ r)}$	width of stiffener	T_{ij}	transformation matrix
$C_{ij}^{\ s}$	weighting coefficients (Eq. (30))	T	kinetic energy
D_{ij}	bending stiffness	T^*	defined by Eq. (39)
$d_{s(or\ r)}$	depth of stiffener	t	time
E	modulus of Young's elasticity	U	strain energy
e	middle surface strain	U^{**}	defined by Eq. (40)
G_{ij}	gyroscope matrix of shell	$u,\ v,\ w$	displacement of shell in x, ϑ and z directions
h	thickness of shell	$U,\ V,\ W$	unknown functions in x, y and z directions (Eq. (36))
$G_{s(or\ r)}$	shear modulus of stringers (or rings)	$u_s,\ v_s,\ w_s$	displacement of stiffeners in x, ϑ and z directions
I	identity matrix	$\vec{V}$	velocity vector
$J_{s(or\ r)}$	polar moment of stiffener	z	distance of a point in stiffener from shell middle surface
K_{ij}	equivalent stiffness matrix	a	cone angle
L	length of shell	β	orientation of fibers
L_{ij}	differential operator (Eq. (28))	$\varkappa$	middle surface curvatures
M_{ij}	mass matrix of shell	ν	Poisson's ratio
M_x	resultant moment in x direction	ε_{sx}	strain of stringers in meridional direction
N	number of grid points	$\varepsilon_{r\vartheta}$	strain of rings in circumferential direction
n	circumferential wave number	ϱ	mass density
N_l	number of layers	ω	natural frequency in rad/s
N_ϑ	initial hoop tension	Π	energy functional
$N_a^{\ x}$	axial load		

They include works by Lam *et al.* on rotating composites and sandwich-type cylindrical shells [4-5], a comparison study on different thin shell theories in addition to a discussion on the effect of boundary conditions on rotating cylindrical shells [6-7]. Chen *et al.* used a nine nodes curvilinear super-parametric finite element to solve problems of vibrations in shells rotating at high speeds about their longitudinal axis [8]. A combined theoretical and experimental study on resonant frequencies and associated mode shapes of truncated conical shells over a wide range of geometrical and modal parameters was carried out by Lindholm and Hu [9]. Lam and Hua analyzed the free vibration of rotating circular conical shell with simply-supported boundary conditions based on Love's first approximation theory [10]. The effect of boundary conditions on free vibration of conical shells, considering the Ritz method, has been studied by Lim and Liew [11].

Although the rotating stiffened conical shell is increasingly being used in many industries, most studies were restricted to the vibration analysis of cylindrical shell. Zhao *et al.* presented the free vibration analysis of simply supported rotating cross-ply laminated cylindrical shells with axial and circumferential stiffeners, using an energy approach [12]. The effects of these stiffeners were evaluated via two methods: stiffeners treated as discrete elements; and stiffeners with properties being averaged over the shell surface by smearing method. Jafari and Bagheri investigated the free vibration analysis of simply supported rotating cylindrical shells with circumferential stiffeners, namely rings with non-uniform eccentricity of stiffeners, and non-uniform spacing distribution of stiffeners [13].

In Spite of the widespread use of stiffened conical shells as a base structures of many industrial processes such as water crafts, drive shafts of gas turbines, high-speed centrifugal separators, motors and rotor systems, a few researches are found on this field [14-22]. Besides, these few researches just focus on non-rotating conical shells and the stiffeners have been modeled using smearing method except the work directed by Talebitooti et al. [22]. They assessed natural frequency of rotating stiffened conical shell in which the stiffeners are modeled by discrete elements. Crenwelge and Muster analyzed conical shells with stringers and rings using an equivalent orthotropic shell model, and compared the frequencies with experimental results [14]. Rao and Reddy studied the optimum design of stiffened conical shells with natural frequency constraint with the aid of averaging method [15]. Langley developed a dynamic stiffness technique to investigate the stiffened shell structures [16]. This method is based on a singly curved orthogonally stiffened shell element having a constant radius of curvature which is simply supported along the curved edges. The stiffeners are taken to be smeared over surface of the element. “Branched shell approach” has been employed by Raj *et al.* to examine the effects of rings on the vibration of conical shells considering both theoretical and experimental methods [17]. Mecitoğlu concentrated on the free vibrations of conical shells with orthogonal stiffeners through the orthotropic material approach [18]. More recently, Goldfeld [19], and Jabareen and Sheinman [20] studied the elastic buckling of stiffened conical shells. Farkas *et al.* analyzed the optimum design of a ring-stiffened conical shell loaded by external pressure with buckling load constraint [21].

All the previous studies used to only deal with stiffened rotating cylindrical shells, rotating non-stiffened conical shells or non-rotating stiffened conical shells while the effects of stiffeners in conical shells were evaluated by an averaging method. Dynamic analysis of rotating stiffened conical shells is rather complex and the common methods used for cylindrical shells are unable to solve

these problems. The Generalized Differential Quadrature Method (GDQM) is an efficient numerical technique which is based on the Differential Quadrature (DQ) method. The mathematical fundamentals and recent developments of the GDQ method as well as its major applications in engineering are discussed in detail by Shu [23]. It is worthwhile to note that the increasing interest of researches [24–31] in this procedure is mainly due to its great simplicity and versatility.

In this paper, the governing equations of motion are a set of partial differential equations with variable coefficients. These fundamental equations are expressed in terms of kinematic parameters and can be extracted by applying Hamilton's principle to the energy function while stiffeners are treated as discrete element. Referring to the formulation for equations of motion and the terms of mid-surface displacements and rotations, the system of second-order linear partial differential equations will be transformed to a set of ordinary differential equations. With the aid of GDQM, governing equations of dynamic equilibrium are transformed to a set of linear algebraic equations. Having imposed the given boundary conditions, numerical eigenvalue equation for the free vibration of the rotating composite conical shell is derived and then solved. Based on the eigensolution, results are obtained to discuss the effect of boundary conditions on the frequency characteristics. Variations of frequency parameter with circumferential wave number are also considered for different rotating velocities. Moreover, it is investigated how the number of stiffeners affects the frequency characteristics. Comparing the results in special cases with those available in the literature and also from FE results, the accuracy of the present analysis will be confirmed.

2 PROBLEM FORMULATION

2.1 Geometrical configuration

The stiffened conical shell, as shown in Fig. 1, is considered to be thin, laminated and composed of an arbitrary number of layers. In this figure, α is the cone angle, L is the length, h is the thickness, a and b are the radii at two ends, and Ω is the constant angular velocity of conical shell about its symmetrical and horizontal axis.

Reference surface of the conical shell is taken to be at its middle surface where an orthogonal co-ordinate system $\left(x,\theta,z\right)$ is fixed, and $r_x = r_x\left(x\right)$ is a radius at any co-ordinate point $\left(x,\theta,z\right)$. Displacement of the shell in x, θ and z directions are denoted by u, v and w, respectively. Depth and width of the stiffeners are symbolized by $d_{s(orr)}$ and $b_{s(orr)}$, respectively and the ring intervals are denoted by s. Subscripts $\left(s,r\right)$ indicate the stringer and ring stiffeners, respectively. Displacements from the middle surface of shell to any point located on the stiffeners are addressed by z.

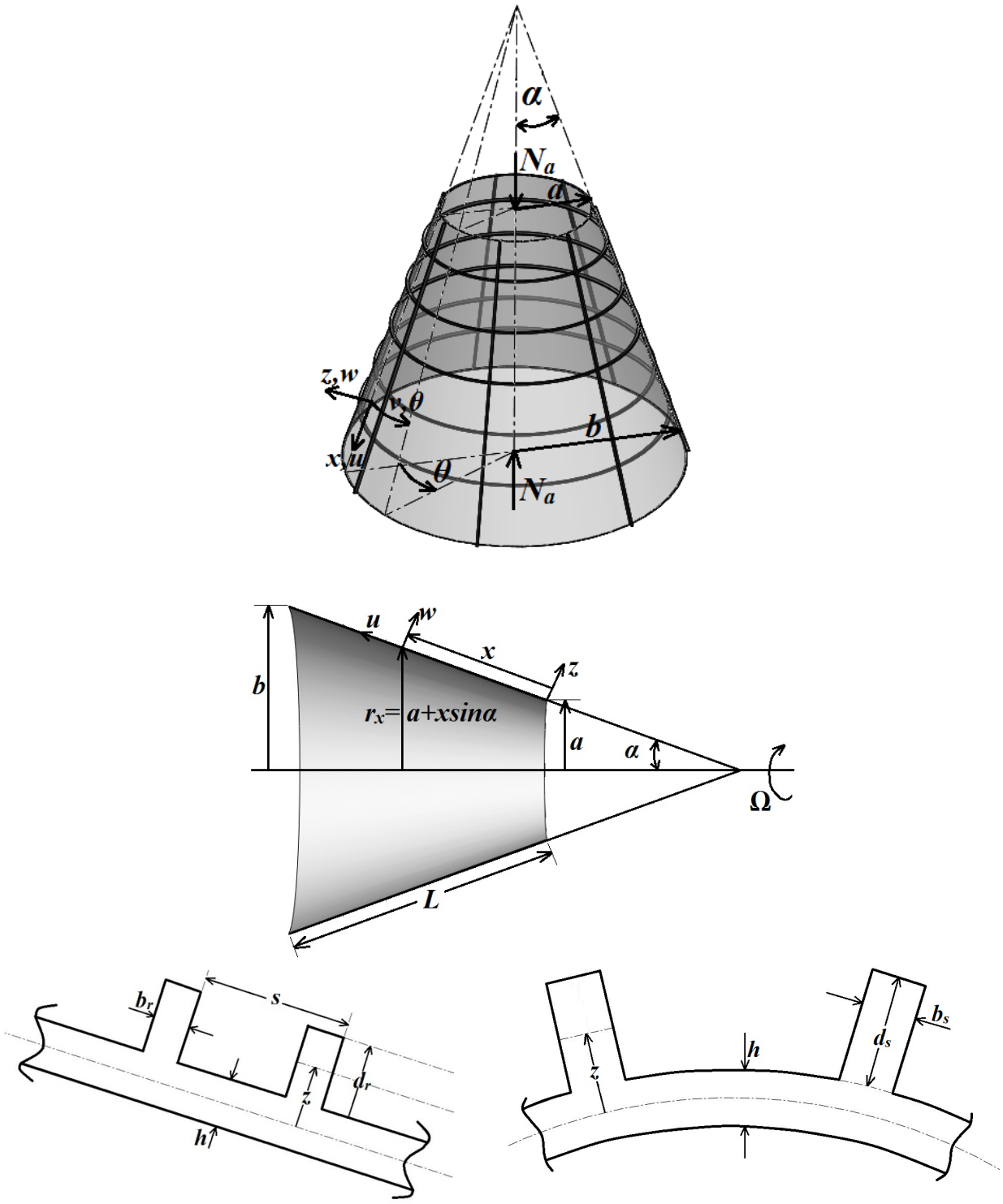

Figure 1 Geometry of stiffened rotating conical shell structure

2.2. Strain energies of shell

The strain energy of the laminated composite conical shell is expressed as:

$$U_{\varepsilon} = \frac{1}{2}\int_{0}^{L}\int_{0}^{2\pi} \varepsilon^{T}\left[S\right]\varepsilon\, r_{x}\, d\theta\, dx \tag{01}$$

where $r_x\left(x\right) = a + x\sin\alpha$ and the strain vector (ε) can be written as:

$$\varepsilon^{T} = \left\{e_1 \quad e_2 \quad e_{12} \quad \kappa_1 \quad \kappa_2 \quad \kappa_{12}\right\} \tag{02}$$

where symbols e_1, e_2 and e_{12} are middle surface strains and symbols κ_1, κ_2 and κ_{12} are middle surface curvatures (the subscripts 1 and 2 denote fiber direction and orthogonal direction, respectively). Geometric relations of deformation for the reference surface of the conical shell can be written as [10]:

$$\begin{gathered} e_1 = \frac{\partial u}{\partial x},\ e_2 = \frac{1}{r_x}\frac{\partial v}{\partial \theta} + \frac{u\sin\alpha + w\cos\alpha}{r_x},\ e_{12} = \frac{1}{r_x}\frac{\partial u}{\partial \theta} + \frac{\partial v}{\partial x} - \frac{v\sin\alpha}{r_x} \\ \kappa_1 = -\frac{\partial^2 w}{\partial x^2}, \quad \kappa_2 = -\frac{1}{{r_x}^2}\frac{\partial^2 w}{\partial \theta^2} + \frac{\cos\alpha}{{r_x}^2}\frac{\partial v}{\partial \theta} - \frac{\sin\alpha}{r_x}\frac{\partial w}{\partial x} \\ \kappa_{12} = 2\left(-\frac{1}{r_x}\frac{\partial^2 w}{\partial x\,\partial \theta} + \frac{\sin\alpha}{{r_x}^2}\frac{\partial w}{\partial \theta} + \frac{\cos\alpha}{r_x}\frac{\partial v}{\partial x} - \frac{v\sin\alpha\cos\alpha}{{r_x}^2}\right) \end{gathered} \tag{03}$$

It is assumed that the displacements are continuous functions of the thickness coordinate, which results in continuous transverse strains.
Meanwhile, stiffness matrix $\left[S\right]$ for a cross-ply laminated shell is given by:

$$\left[S\right] = \begin{bmatrix} A_{11} & A_{12} & A_{16} & B_{11} & B_{12} & B_{16} \\ A_{21} & A_{22} & A_{26} & B_{21} & B_{22} & B_{26} \\ A_{61} & A_{62} & A_{66} & B_{61} & B_{62} & B_{66} \\ B_{11} & B_{12} & B_{16} & D_{11} & D_{12} & D_{16} \\ B_{21} & B_{22} & B_{26} & D_{21} & D_{22} & D_{26} \\ B_{61} & B_{62} & B_{66} & D_{61} & D_{62} & D_{66} \end{bmatrix} \tag{04}$$

where $A = [A_{ij}]$, $B = [B_{ij}]$ and $D = [D_{ij}]$ $\left(i, j = 1, 2, 6\right)$ are extensional, coupling and bending stiffness matrices, respectively. For an arbitrary laminated composite shell, they can be rewritten as:

$$A_{ij} = \sum_{k=1}^{N_l} \overline{Q}_{ij}^{k}(h_k - h_{k+1})$$
$$B_{ij} = \frac{1}{2}\sum_{k=1}^{N_l} \overline{Q}_{ij}^{k}(h_k^2 - h_{k+1}^2) \tag{05}$$
$$D_{ij} = \frac{1}{3}\sum_{k=1}^{N_l} \overline{Q}_{ij}^{k}(h_k^3 - h_{k+1}^3)$$

where N_l is the total number of layers in the laminated composite conical shell. Parameters h_k and h_{k+1} denote distance from the shell reference surface to the outer and inner surface of k^{th} layer as shown in Fig. 2.

$\overline{Q}_{ij}^{k}$ is the element of transformed reduced stiffness matrix for the k^{th} layer and it is defined as:

$$\overline{Q}^{k} = T^{-1}Q^{k}T \tag{06}$$

where $\left[T\right]$ is transformation matrix of the principal material coordinate and the shell coordinates system, and is defined as [3]:

$$\left[T\right] = \begin{bmatrix} \cos^2\beta & \sin^2\beta & 2\cos\beta\sin\beta \\ \sin^2\beta & \cos^2\beta & -2\cos\beta\sin\beta \\ -\cos\beta\sin\beta & \cos\beta\sin\beta & \cos^2\beta - \sin^2\beta \end{bmatrix} \tag{07}$$

where β is orientation of the fibers and $\left[Q\right]$ is reduced stiffness matrix defined as:

$$\left[Q\right] = \begin{bmatrix} Q_{11} & Q_{12} & 0 \\ Q_{21} & Q_{22} & 0 \\ 0 & 0 & Q_{66} \end{bmatrix} \tag{07}$$

Moreover, material constants in the reduced stiffness matrix $\left[Q\right]$ are defined as:

$$Q_{11} = \frac{E_{11}}{1-\upsilon_{12}\upsilon_{21}}\ ,\ Q_{12} = Q_{21} = \frac{\upsilon_{12}E_{22}}{1-\upsilon_{12}\upsilon_{21}}\ ,$$
$$Q_{22} = \frac{E_{22}}{1-\upsilon_{12}\upsilon_{21}}\ ,\ Q_{66} = G_{12} \tag{09}$$

where E_{11} and E_{22} are the elastic moduli, G_{12} is the shear modulus, and υ_{12} and υ_{21} are the Poisson's ratios.

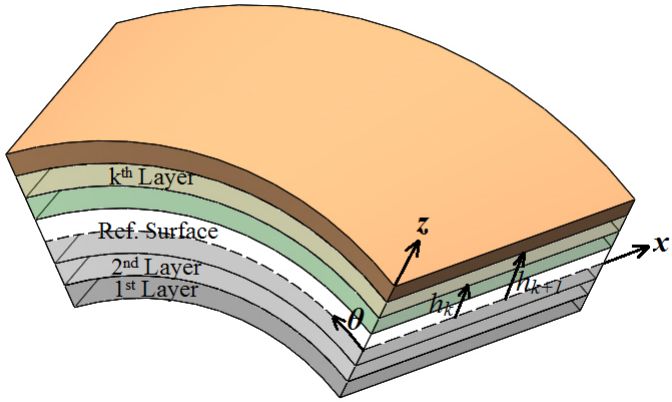

Figure 2 Cross-sectional view of the laminated conical shell

It should be noted that the work is carried out on the shell due to centrifugal force generated by rotation. The work done on the shell can be written as [22]:

$$U_h = \frac{1}{2}\int_0^L \int_0^{2\pi} N_\theta \left[\left(\frac{v\cos\alpha}{r_x} - \frac{1}{r_x}\frac{\partial w}{\partial \theta} \right)^2 + \left(\frac{1}{r_x}\frac{\partial v}{\partial \theta} + \frac{w\cos\alpha}{r_x} \right)^2 \right] r_x dx d\theta \tag{10}$$

where N_q is the initial hoop stress due to centrifugal force which is given by:

$$N_\theta = \rho h \Omega^2 r_x^2 (x) \tag{11}$$

Besides, the work done on the shell due to axial forced is described as:

$$U_{N_a} = N_a^x \int_0^{2\pi} \int_0^L \frac{1}{2}\left(\frac{\partial w}{\partial x} \right)^2 r(x,z)\, dx\, d\theta \tag{12}$$

where N_a^x is the axial load on edge of shell in x direction. The effect of N_a^θ and N_a^z are null for both simply supported and clamped boundary conditions [32].

2.3 Kinetic energy of the shell

Kinetic energy of the rotating conical shell is expressed as:

$$T_{sh} = \frac{1}{2}\rho h \int_0^{2\pi}\int_0^{L} \vec{V}.\,\vec{V}\, r_x\, dx\, d\theta \tag{13}$$

where $\vec{V}$ is the velocity vector at any point of the shell given by:

$$\vec{V} = \dot{\vec{r}} + \left(\Omega\cos\alpha\,\vec{i} - \Omega\sin\alpha\,\vec{k}\right)\times\vec{r} \tag{14}$$

Here, $\left(\cdot\right)$ presents differentiation with respect to time.

In Eq. (14) the displacement vector is written as:

$$\vec{r} = u\vec{i} + v\vec{j} + w\vec{k} \tag{15}$$

where $\vec{i}$, $\vec{j}$ and $\vec{k}$ respectively denote the unit vectors in x, θ and z directions for nonrotating frame.

Having substituted Eqs. (14) and (15) into Eq. (13), the kinetic energy expression of the shell can be expanded in the form below:

$$T_{sh} = \frac{1}{2}\rho h \int_0^{2\pi}\int_0^{L} \left\{ \begin{array}{l} \left[\dot{u}^2 + \dot{v}^2 + \dot{w}^2\right] + \Omega^2\left[v^2 + \left(w\cos\alpha + u\sin\alpha\right)^2\right] \\ +2\Omega\sin\alpha\left[\dot{v}u - \dot{u}v\right] + 2\Omega\cos\alpha\left[\dot{v}w - \dot{w}v\right] \end{array} \right\} r_x\, dx\, d\theta \tag{16}$$

2.4 Stiffener energies

The stiffener-to-shell joints are the significant technology issues, either adhesively bonded or mechanically fastened to the shell or more recently fabricated without fasteners by co-curing the stringers and co-bonding the rings. In all of the abovementioned technologies the shell and the stiffener have same displacements. Therefore, the stiffeners (rings and stringers) are assumed to be an integral part of the shell. Meanwhile, when stiffeners of equal strength are closely and evenly spaced, the stiffened shell can be modeled as an equivalent orthotropic shell (smearing method). However, as the stiffener spacing increases or the wavelength of vibration becomes smaller than the stiffener spacing, determination of dynamic characteristics for the stiffened shell cannot be accurate anymore. Thus, a more general model needs the stiffeners to be treated as discrete elements. When modeled in this respect, it is advantageous to use non-uniform eccentricity, unequally spaced and different materials for stiffener stiffeners. In order to maintain displacement compatibility between the stiffeners and the stiffened shell, a special transformation is used which includes coupling effects due to eccentric placement of the stiffener. It should be also noted that the displacements vary through depth of the stiffeners. Therefore, displacement of a point at distance z from the shell middle surface can be explained by shell displacement function [15]:

$$u_{s(orr)} = u - z\frac{\partial w}{\partial x}\ ,\ v_{s(orr)} = v - \frac{z}{r_x}\frac{\partial w}{\partial \theta}\ ,\ w_{s(orr)} = w - \frac{z}{r_x}\frac{\partial v}{\partial \theta} \tag{17}$$

The strain of stringers in the meridional direction and the strain of rings in the circumferential direction are respectively defined as:

$$\varepsilon_{sx} = \frac{\partial u}{\partial x} - z\frac{\partial^2 w}{\partial x^2} \tag{18}$$

$$\varepsilon_{r\theta} = \frac{1}{r_x}\left(\frac{\partial v}{\partial \theta} - \frac{z}{r_x}\frac{\partial^2 w}{\partial \theta^2} + u\sin\alpha - z\sin\alpha\frac{\partial w}{\partial x} + w\cos\alpha - \frac{z\cos\alpha}{r_x}\frac{\partial v}{\partial \theta}\right) \tag{19}$$

Using discrete stiffener theory, the strain energy for the stringer can be written as [22]:

$$\begin{aligned} U_s &= \frac{1}{2}\sum_{k=1}^{N_s} E_{sk}\int_0^L\int_{A_{sk}} \varepsilon_{sx}^2\, dA_{sk}\, dx \\ &+\frac{1}{2}\sum_{k=1}^{N_s} G_{sk}J_{sk}\int_0^L\left[\frac{1}{r_{xk}^2}\frac{\partial^2 w_s}{\partial x\,\partial\theta} - \frac{2\sin\alpha}{r_{xk}^2}\frac{\partial w}{\partial \theta} - \frac{\cos\alpha}{r_{xk}}\frac{\partial v}{\partial x} + \frac{2\sin\alpha\cos\alpha}{r_{xk}^2}v\right]^2 dx \end{aligned} \tag{20}$$

where $G_{sk}J_{sk}$ and A_{sk} are torsional stiffness and cross sectional area of the k^{th} stringer, respectively, with N_s being the number of stringers.

The strain energy of the ring can be written as [22]:

$$U_r = \frac{1}{2}\sum_{k=1}^{N_r} E_{rk}\int_0^{2\pi}\int_{A_{rk}} \varepsilon_{r\theta}^2\, dA_{rk}r_{xk}\, d\theta + \frac{1}{2}\sum_{k=1}^{N_r} G_{rk}J_{rk}\int_0^{2\pi}\left[\frac{1}{r_{xk}^2}\left(\frac{\partial^2 w_s}{\partial\theta\,\partial x}\right)^2\right] r_{xk}d\theta \tag{21}$$

where $G_{rk}J_{rk}$ and A_{rk} are torsional stiffness and cross sectional area of the k^{th} ring, respectively, while N_r is the number of rings.

The kinetic energy for stringers and rings may be written as:

$$T_s = \frac{1}{2}\rho_{sk}\sum_{k=1}^{N_s}\int_0^L\int_{A_{sk}}\begin{bmatrix} \dot{u}_s^2 + \dot{v}_s^2 + \dot{w}_s^2 + \Omega^2 v_s^2 \\ +2\Omega\sin\alpha\left(\dot{v}_s u_s - \dot{u}_s v_s\right) \\ +2\Omega\cos\alpha\left(\dot{v}_s w_s - \dot{w}_s v_s\right) \\ +\Omega^2\left(w_s\cos\alpha + u_s\sin\alpha\right)\end{bmatrix} dA_{sk}dx \tag{22}$$

$$T_r = \frac{1}{2}\rho_{rk}\sum_{k=1}^{N_r}\int_0^{2\pi}\int_{A_{rk}}\begin{bmatrix}\dot{u}_r^2+\dot{v}_r^2+\dot{w}_r^2+\Omega^2 v_r^2\\ +2\Omega\sin\alpha\left(\dot{v}_r u_r-\dot{u}_r v_r\right)\\ +2\Omega\cos\alpha\left(\dot{v}_r w_r-\dot{w}_r v_r\right)\\ +\Omega^2\left(w_r\cos\alpha+u_r\sin\alpha\right)\end{bmatrix} r_{xk}dA_{rk}d\theta \tag{23}$$

where $\rho_{s(or\,r)k}$ is density of the k^{th} stringer (or ring).

In the case of stringers, the hoop stress created due to centrifugal force is negligible. However, the work done on the ring by this hoop stress can be calculated in a similar way to that of the shell itself. Therefore, the work expressions for the stringer and ring would be:

$$U_{sh} = 0 \tag{24}$$

$$U_{rh} = \frac{1}{2}\sum_{k=1}^{N_r}\int_0^{2\pi}\int_{A_{rk}} N_\theta\begin{bmatrix}\left(\dfrac{v_r\cos\alpha}{r_x}-\dfrac{1}{r_x}\dfrac{\partial w_r}{\partial\theta}\right)^2\\ +\left(\dfrac{1}{r_x}\dfrac{\partial v_r}{\partial\theta}+\dfrac{w_r\cos\alpha}{r_x}\right)^2\end{bmatrix} r_{xk}dA_{rk}d\theta \tag{25}$$

2.5. Governing Equations of motion

The governing differential equations of motion can be derived using Hamilton's principle:

$$\int_{t_1}^{t_2}\left(\delta\Pi\right)dt = 0 \tag{26}$$

where $\delta\Pi$ is variation of the energy functional and t denotes the time. The energy functional of a stiffened rotating conical shell can thus be written as:

$$\Pi = T + T_r + T_s - U_h - U_\varepsilon - U_s - U_r - U_{rh} - U_{N_a} \tag{27}$$

Substituting Eqs. (1), (10), (12), (16), (20-23) and (25) into Eq. (27), followed by applying Hamilton's principle to the energy function yields the matrix relationship below:

$$\begin{bmatrix}L_{11} & L_{12} & L_{13}\\ L_{21} & L_{22} & L_{23}\\ L_{31} & L_{32} & L_{33}\end{bmatrix}\begin{Bmatrix}u\\ v\\ w\end{Bmatrix} = 0 \tag{28}$$

where the coefficients $L_{ij}\left(i,j=1,2,3\right)$ are differential operators of $\begin{Bmatrix}u & v & w\end{Bmatrix}^T$.

2.6 Assumed-mode method and GDQM solution of the governing equations

The GDQM is based on a simple mathematical concept that any sufficiently smooth function in a domain can be expressed approximately as an $\left(N-1\right)^{th}$ order polynomial in the overall domain. In other words, at a discrete mesh point in a domain, the derivative of a sufficiently smooth function with respect to a coordinate direction can be approximated by taking a weighted linear sum of the functional values at all discrete mesh points in coordinate direction. Thus the partial derivatives of a function $f(x_i,\theta_i)$ as an example, at a point (x_i,q_i) are expressed as [23]:

$$\left.\frac{\partial^s f\left(x,\theta\right)}{\partial x^s}\right|_{x=x_i}=\sum_{j=1}^{N}C_{ij}^{s}f\left(x_i,\theta_j\right)\ ,\quad i=1,2,...,N. \tag{29}$$

where N is the number of grid points and f can be taken as either u, v or w; and parameters of C_{ij}^{s} are respective weighting coefficients related to the s^{th} order derivatives which are obtained as follows:

If $s=1$, namely for the first order derivative, then:

$$C_{ij}^{1}=\frac{M^{(1)}\left(x_i\right)}{\left(x_i-x_j\right)M^{(1)}\left(x_j\right)}\quad for\ i\neq j\ and\ i,j=1,2,...N \tag{30}$$

and:

$$C_{ii}^{1}=-\sum_{j=1\left(j\neq i\right)}^{N}C_{ij}^{1}\quad for\ \ i=1,2,...,N \tag{31}$$

where $M^{(1)}\left(x\right)$ is the first derivative of $M\left(x\right)$ and can be defined as:

$$M\left(x\right)=\prod_{j=1}^{N}\left(x-x_j\right)\quad M^{(1)}\left(x_k\right)=\prod_{j=1\left(j\neq k\right)}^{N}\left(x_k-x_j\right) \tag{32}$$

If $s>1$, namely for second and higher order derivatives, the weighting coefficients are obtained using the following simple recurrence relationship:

$$C_{ij}^{s}=r\left(C_{ij}^{1}\cdot C_{ii}^{s-1}-\frac{C_{ij}^{s-1}}{x_i-x_j}\right)for\ i\neq j\,and\,i,j=1,2,...,N;\quad s=2,3,...,N-1 \tag{33}$$

and:

$$C_{ii}^{s} = -\sum_{j=1(j\neq i)}^{N} C_{ij}^{s} \quad for\ i = 1,2,...,N \tag{34}$$

Since the coordinate distribution and the number of discrete grid points can be arbitrarily chosen in the implementation of GDQM, following distributions of the grid points toward meridional x direction will be used in this formulation:

$$x_i = \frac{i-1}{N-1} L \ , \ i = 1,2,...,N \tag{35}$$

It is noteworthy that the grid points should be distributed in such a way that one grid point is provided in every ring location.

Vibration modes of the laminated circular conical shell are characterized by n, the number of circumferential waves and the natural frequency, ω. A general expression for displacement field is assumed to have the form of a product with unknown continuous smooth functions in the meridional direction and trigonometric function along the circumferential direction, that is to say [27]:

$$\begin{aligned} u(x,\theta,t) &= U(x)\cos(n\theta + \omega t) \\ v(x,\theta,t) &= V(x)\sin(n\theta + \omega t) \\ w(x,\theta,t) &= W(x)\cos(n\theta + \omega t) \end{aligned} \tag{36}$$

By substituting the displacement field (36) into the set of partial differential governing equations (28) in temporal-spatial domain, a set of ordinary differential equations with variable coefficients toward meridional x direction is produced as:

$$T^{*}\,\mathbf{U}^{*} = 0 \tag{37}$$

where $\mathbf{U}^{*T} = \{ U(x), V(x), W(x) \}$ is an unknown spatial function vector of mode shape which describes the distribution of vibrational amplitude in meridional x direction, while $T^{*} = \left[T_{ij}^{*}\right], (i,j = 1,2,3)$ is a 3×3 differential operator matrix of $\mathbf{U}^{*}$ and is defined as:

$$T^{*} = \begin{bmatrix} M_{11} & M_{12} & M_{13} \\ M_{21} & M_{22} & M_{23} \\ M_{31} & M_{32} & M_{33} \end{bmatrix} \omega^2 + \begin{bmatrix} G_{11} & G_{12} & G_{13} \\ G_{21} & G_{22} & G_{23} \\ G_{31} & G_{32} & G_{33} \end{bmatrix} \omega + \begin{bmatrix} K_{11} & K_{12} & K_{13} \\ K_{21} & K_{22} & K_{23} \\ K_{31} & K_{32} & K_{33} \end{bmatrix} \tag{38}$$

where coefficients of $M_{i,j}$,$G_{i,j}$ and $K_{i,j}\left(i,j=1,2,3,4,5\right)$ are given in detail in Appendix A.

With imposing Eq. (29) on Eq. (37) and rearrangement of the Eq. (37) with respect to the order of derivative, the approximate governing equations in the form of linear discrete algebraic equations are obtained as follows:

$$T^{*}\,\mathbf{U}^{*}\Big|_{x=x_i}=\mathbf{R}_{5X15}\,\mathbf{U}^{**}_{15X1}\Big|_{x=x_i}=0\ \left(i=1,2,3,...,N\right) \tag{39}$$

where N is the number of total discrete grid points in meridional x direction and $\mathbf{U}^{**}$ is given by:

$$\begin{aligned}\mathbf{U}^{**\mathbf{T}}\Big|_{x=x_i}=\{&U\left(x_i\right),U^{(1)}\left(x_i\right),U^{(2)}\left(x_i\right),U^{(3)}\left(x_i\right),U^{(4)}\left(x_i\right),\\&V\left(x_i\right),V^{(1)}\left(x_i\right),V^{(2)}\left(x_i\right),V^{(3)}\left(x_i\right),V^{(4)}\left(x_i\right),\\&W\left(x_i\right),W^{(1)}\left(x_i\right),W^{(2)}\left(x_i\right),W^{(3)}\left(x_i\right),W^{(4)}\left(x_i\right)\}\end{aligned} \tag{40}$$

where:

$$\begin{aligned}U^{(s)}\left(x_i\right)&=\sum_{j=1}^{N}C_{ij}^{s}U\left(x_j\right),\\V^{(s)}\left(x_i\right)&=\sum_{j=1}^{N}C_{ij}^{s}V\left(x_j\right),\\W^{(s)}\left(x_i\right)&=\sum_{j=1}^{N}C_{ij}^{s}W\left(x_j\right),\ \ \left(s=1,2,3,4\right)\end{aligned} \tag{41}$$

Thus, the whole system of differential equation has been discretized and the the following set of linear algebraic equations will be produced from general combination of these equations:

$$\left\{\left[M\right]\omega^{2}\right\}\left\{d\right\}+\left\{\left[G\right]\omega\right\}\left\{d\right\}+\left[K_{dd}\right]\left\{d\right\}+\left[K_{db}\right]\left\{b\right\}=0 \tag{42}$$

In the above equations, vectors $\left\{d\right\}$ and $\left\{b\right\}$ with dimensions $3N$ - 8 and 8, denote the unknowns at the sampling points within interior domain and those on the boundary, respectively and can be written as:

$$\begin{aligned}\left\{d\right\}^{T}=\{&U\left(x_2\right),U\left(x_3\right),...,U\left(x_{N-2}\right),U\left(x_{N-1}\right),\\&V\left(x_2\right),V\left(x_3\right),...,V\left(x_{N-2}\right),V\left(x_{N-1}\right),\\&W\left(x_3\right),W\left(x_4\right),...,W\left(x_{N-3}\right),W\left(x_{N-2}\right)\}^{T}\end{aligned} \tag{43}$$

$$\begin{aligned}\{b\}^T = \{&U(x_1),V(x_1),W(x_1),W(x_2),\\ &U(x_N),V(x_N),W(x_{N-1}),W(x_N)\}^T\end{aligned} \tag{44}$$

The dimensions of $[M]$, $[K_{dd}]$ and $[G]$ are $(3N-8)\times(3N-8)$ and dimension of $[K_{db}]$ is $(3N-8)\times 8$.

Similarly, discretized form of the boundary conditions becomes:

$$[K_{bd}]\{d\}+[K_{bb}]\{b\}=0 \tag{45}$$

The dimension of $[K_{bd}]$ is $8\times(3N-8)$ and dimension of $[K_{bb}]$ is 8×8.

In current application of GDQM, five boundary conditions are considered for rotating conical shells, namely:

a) Clamped at both edges (Cs-Cl):

$$u=0,\ v=0,\ w=0,\ \frac{\partial w}{\partial x}=0 \quad at\, x=0 \text{ and } L \tag{46}$$

b) Simply supported at both edges (Ss-Sl):

$$v=0,\ w=0,\ N_x=0,\ M_x=0 \quad at\, x=0 \text{ and } L \tag{47}$$

c) Simply supported at small edge - clamped at large edge (Ss-Cl):

$$\begin{aligned}&v=0,\ w=0,\ N_x=0,\ M_x=0 \ \ at\, x=0\\ &u=0,\ v=0,\ w=0,\ \frac{\partial w}{\partial x}=0 \quad at\, x=L\end{aligned} \tag{48}$$

d) Clamped at small edge - simply supported at large edge (Cs-Sl):

$$\begin{aligned}&u=0,\ v=0,\ w=0,\ \frac{\partial w}{\partial x}=0 \ \ at\, x=0\\ &v=0,\ w=0,\ N_x=0,\ M_x=0 \quad at\, x=L\end{aligned} \tag{49}$$

e) Free at both edges (Fs-Fl):

$$N_x=0,\ N_{x\theta}=,\ M_x=0,\ M_{x\theta}=0 \ \ at\, x=0 \text{ and } L \tag{50}$$

Using Eq. (45) to eliminate boundary degrees of freedom $\{b\}$ from Eq. (44), it can be concluded that:

$$\left\{[M]\omega^2\right\}\{d\}+\left\{[G]\omega\right\}\{d\}+\left\{[K_{dd}]-[K_{db}][K_{bb}]^{-1}[K_{bd}]\right\}\{d\}=0 \tag{51}$$

Eq. (51) is a non-standard eigenvalue equation. For a given frequency, it can be equivalently transformed into a standard form of eigenvalue equation as [27]:

$$\left(\underbrace{\begin{bmatrix}0 & I\\ -K & -G\end{bmatrix}}_{A^*}-\underbrace{\begin{bmatrix}I & 0\\ 0 & M\end{bmatrix}}_{B^*}\omega\right)\begin{Bmatrix}d\\ \omega d\end{Bmatrix}=0 \tag{52}$$

where I is a $(3N-8)\times(3N-8)$ identity matrix.

Using a conventional eigenvalue approach, the standard eigenvalue equation (52) can be solved, and $(6N-16)$ eigenvalues are obtained. From these eigenvalues, the two eigenvalues are chosen for which the absolute of real values are the smallest. One of these eigenvalues is negative and corresponds to backward wave, and the other one is positive and corresponds to forward wave. In the case of a stationary conical shell, these two eigenvalues are identical and the vibration of the conical shell is a standing wave motion.

3 NUMERICAL RESULTS

In the presentation of results shown by figures, the backward and forward waves are presented as a solid line and a dashed line, respectively, with the unit of rotating speed W being in rps (revolutions per second). In addition, five boundary conditions are considered here for the rotating conical shell. These boundary conditions include fully clamped (Cs-Cl), fully simply supported (Ss-Sl), fully unsupported (Fs-Fl), simply supported at small edge - clamped at large edge (Ss-Cl), and clamped at small edge - simply supported at large edge (Cs-Sl). Material properties of the shells used in this study are given in Table 1. In addition, unless otherwise stated, geometrical dimensions and material properties of the stiffeners used in the present study are given in Table 2.

Table 1 Mechanical properties of the material

	Modulus of Elasticity (GPa)	Poisson's Ratio	Modulus of Rigidity (GPa)	Density (kg/m^3)
Isotropic	E=7.6	υ=0.3	G=2.9	ρ=1643
Orthotropic	E_{22}=7.6 E_{11}=2.5 E_{22}	υ_{12}=0.26	G_{12}=4.1	ρ=1643

Table 2 Geometrical parameters and material properties of the stiffeners used in this study

Stiffener Type	***Stringer***	***Ring***
Depth (mm)	*8*	*8*
Width (mm)	*2*	*2*
E (N/m^2)	$3.0E_{11}$	$3.0E_{11}$
υ	*0.3*	*0.3*
$r\,(kg\,/\,m^3)$	*1643*	*1643*

The GDQM is especially suitable for considering global characteristics such as free vibration or buckling analyses. Numerical accuracy of the GDQM, with excellent weighting characteristics, is highly reliable, and its implementation is both simple and efficient. To show versatility and efficiency of the present analysis, three comparisons are made with the available results in the existing literature. The initial comparisons are made with Refs. [33-34] for a non-rotating conical shell with Ss-Sl boundary condition and also the one with Cs-Cl boundary condition by taking Ω=0 into the present formulations as shown in Table 3 and Table 4, respectively.

Table 3 Comparison of frequency parameter $f = \omega b\sqrt{\left(1-\upsilon^2\right)\rho\,/\,E}$ for a non-rotating isotropic conical shell with Ss-Sl boundary condition (m=1, υ=0.3, h/b=0.01, Lsinα/b=0.25)

	α=30°				**α=45°**			
n	**Irie [33]**	**LAM [34]**	**Present (GDQM)**	**Present (ABAQUS)**	**Irie [33]**	**LAM [34]**	**Present (GDQM)**	**Present (ABAQUS)**
2	0.7910	0.8420	0.8405	0.7907	0.6879	0.7655	0.7639	0.6874
3	0.7248	0.7376	0.7374	0.7280	0.6973	0.7212	0.7204	0.6965
4	0.6352	0.6362	0.6367	0.6345	0.6664	0.6739	0.6738	0.6652
5	0.5531	0.5528	0.5535	0.5519	0.6304	0.6323	0.6327	0.6286
6	0.4949	0.4950	0.4955	0.4932	0.6032	0.6035	0.6041	0.6007
7	0.4653	0.4661	0.4663	0.4630	0.5918	0.5921	0.5926	0.5884
8	0.4654	0.4660	0.4656	0.4614	0.5992	0.6001	0.6003	0.5948
9	0.4892	0.4916	0.4907	0.4855	0.6257	0.6273	0.6272	0.6203

Table 4 Comparison of frequency parameter $f = \omega b\sqrt{\left(1 - \upsilon^2\right)\rho / E}$ for a non-rotating isotropic conical shell with Cs-Cl boundary condition (m=1, υ=0.3, h/b=0.01, Lsinα/b=0.5)

	$\alpha=45^o$				$\alpha=60^o$			
n	**Irie [33]**	**LAM [34]**	**Present (GDQM)**	**Present (ABAQUS)**	**Irie [33]**	**LAM [34]**	**Present (GDQM)**	**Present (ABAQUS)**
1	0.8120	0.8452	0.8128	0.8117	0.6316	0.6449	0.6324	0.6312
2	0.6696	0.6803	0.6713	0.6693	0.5523	0.5568	0.5535	0.5520
3	0.5430	0.5553	0.5449	0.5425	0.4785	0.4818	0.4798	0.4780
4	0.4570	0.4778	0.4588	0.4561	0.4298	0.4361	0.4308	0.4290
5	0.4095	0.4395	0.4108	0.4093	0.4093	0.4202	0.4098	0.4082
6	—	—	0.3959	0.3954	—	—	0.4113	0.4144
7	—	—	0.4054	0.4131	—	—	0.4385	0.4447
8	—	—	0.4442	0.4553	—	—	0.4834	0.4949
9	—	—	0.5033	0.5157	—	—	0.5496	0.5611

The secondary comparisons are listed in Tables 5-6 in order to verify the natural frequencies using GDQ and FE techniques for non-rotating stiffened isotropic conical shell of fully clamped and simply supported boundary conditions, respectively. Stiffened shell is modeled with the aid of commercial FEM software ABAQUS, in which elements of S8R and C3D20R types are used to model the shell and stiffeners, respectively.

Table 5 Comparison of frequency for a non-rotating stiffened isotropic conical shell with Cs-Cl boundary condition (m=1, υ=0.3, h=2mm, L=1m, a=0.5m, $\alpha=20^o$)

	$N_r=5$, $N_s=0$		$N_r=0$, $N_s=6$		$N_r=4$, $N_s=6$	
n	**Present (GDQM)**	**Present (ABAQUS)**	**Present (GDQM)**	**Present (ABAQUS)**	**Present (GDQM)**	**Present (ABAQUS)**
1	357.22	355.71	338.53	337.15	339.89	340.72
2	246.71	245.50	248.90	248.14	246.00	245.13
3	177.73	176.69	178.26	179.82	176.17	177.20
4	134.10	133.24	134.71	134.53	133.46	133.12
5	105.86	105.31	105.03	104.83	105.05	105.13
6	88.317	88.412	84.391	84.449	86.55	87.764
7	79.483	80.668	71.834	71.541	77.58	79.515
8	78.166	80.655	64.354	64.074	75.31	78.712
9	82.785	86.295	61.4068	61.195	78.51	83.660

Table 6 Comparison of frequency for a non-rotating stiffened isotropic conical shell with Ss-Sl boundary condition (m=1, υ=0.3, h=2mm, L=1m, a=0.5m, α=20°)

n	N_r=5, N_s=0		N_r=0, N_s=6		N_r=4, N_s=6	
	Present (GDQM)	Present (ABAQUS)	Present (GDQM)	Present (ABAQUS)	Present (GDQM)	Present (ABAQUS)
2	234.98	232.33	237.52	236.02	234.39	231.75
3	151.89	148.56	152.66	151.59	150.57	149.01
4	102.71	99.618	103.32	101.07	102.25	99.751
5	74.94	72.498	73.844	71.681	74.309	72.429
6	61.42	60.240	56.535	54.856	59.902	59.587
7	58.54	59.097	48.299	46.504	56.446	57.689
8	63.13	65.204	45.944	44.378	60.002	63.096
9	71.92	74.750	47.856	47.207	67.588	72.336

The third comparison, as depicted in Fig. 3, is related to a rotating stiffened laminated cylindrical shell with fully simply supported boundary condition by taking α=0 into the present formulations.

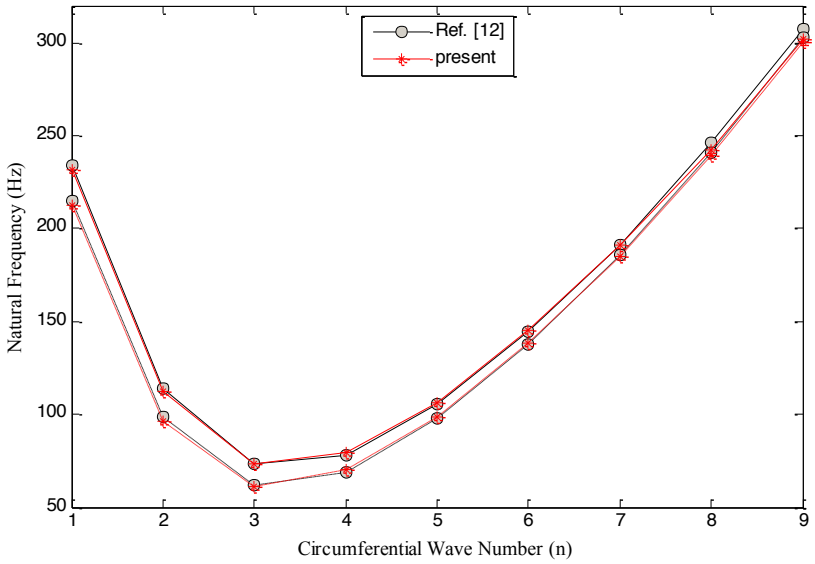

Figure 3 Variation of natural frequencies for the rotating orthogonally stiffened composite cylindrical shell with circumferential wave number in comparison between results of the present study and those reported in Ref. [12]. (L=2m, a=0.5m, h=2.5mm, m=1, Ω=10rev/s, N_s=5, N_r=15, [0°/90°/0°])

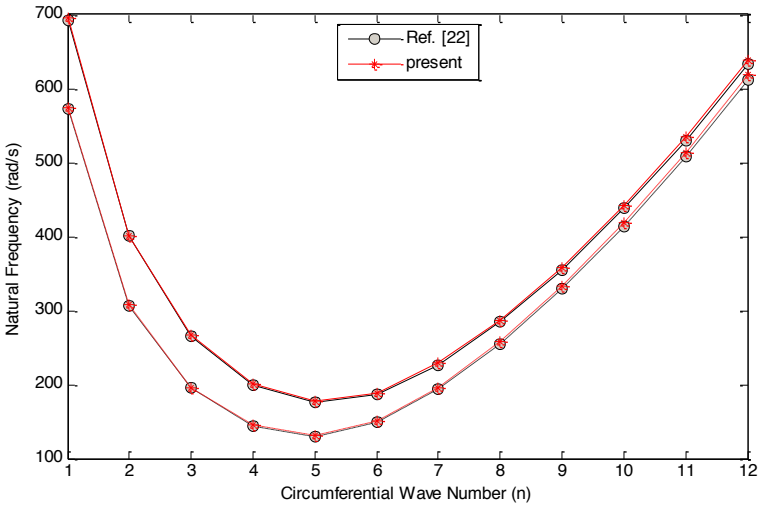

Figure 4 Variation of natural frequencies for the rotating orthogonally stiffened composite conical shell with circumferential wave number in comparison between results of the present study and those reported in Ref. [22]. (L/a=10, h/a=0.002, α=15°, m=1, Ω=10rev/s, N_s=20, N_r=10, [0°/90°/0°])

The last comparison is made with Ref. [22] for a rotating stiffened laminated conical shell being simply supported at both edges as shown in Fig. 4. With numerical comparisons shown in Tables 3-6 and Figs. 3-4, it is evident that the presented results are in a good agreement with the data available in the literature and FE results, which demonstrates accuracy of the current work. In addition, the computed frequency parameter $f = \omega b\sqrt{\rho\left(1-\upsilon^2\right)/E}$ for non-rotating un-stiffened isotropic conical shell with free boundary conditions were compared to those obtained experimentally from Ref. [9] as shown in Fig(5). Comparing the present results with those of experiments reveals an excellent agreement. The slight divergence is attributed to satisfaction of the assumed boundary conditions among these two methods.

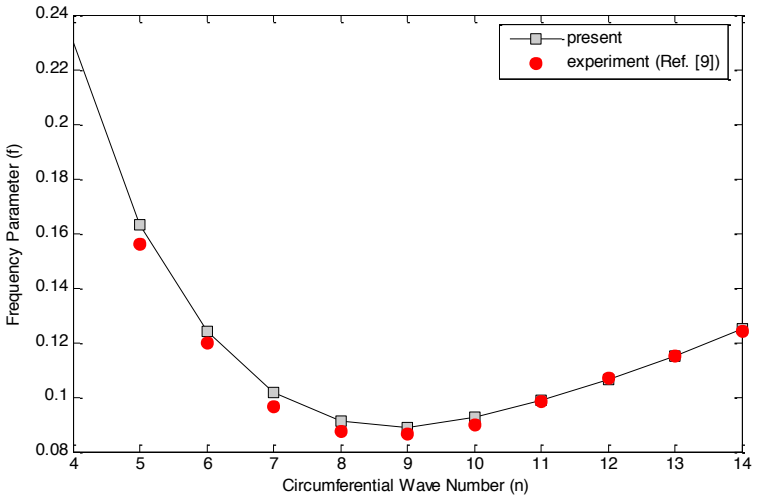

Figure 5 Variation of natural frequencies for the un-stiffened isotropic conical shell with circumferential wave number in comparison between results of the present study and those reported in Ref. [9]. (L/a=2.53, h/a=0.00127, α=30.2°, m=1, Ω=0rev/s)

In Fig. (6), an additional comparison is made between the theoretically and experimentally produced natural frequencies of orthogonal stiffened non-rotating conical shell by Ref. [14] and the theory proposed here. The present theory estimates more accurate results than the smearing method, since the former assumes the stiffeners as discrete elements while the latter considers the properties of the stiffeners averaged throughout the shell. Moreover, the present theory is in good agreement with the experimental results. In higher modes ($n \geq 8$) the difference is occurred between the present theory and the experimental results. This seems to occur because the shell stiffened with widely separated stiffeners is less rigid upon bending than expected before. On the other hand, in present method the stiffener is expected to be moved with structure as an integral part which may be different from a real structure in experiments. There may be also some other parameters such as the effects of boundary condition and the errors of experimental setup which cause discrepancy. However, the present method is found more reliable than the smearing method. There is just 10% of discrepancy comparing the present work with those of experiment, whereas the inconsistency of 41% was presented by Ref. [14], comparing the experimental results with those of smearing method.

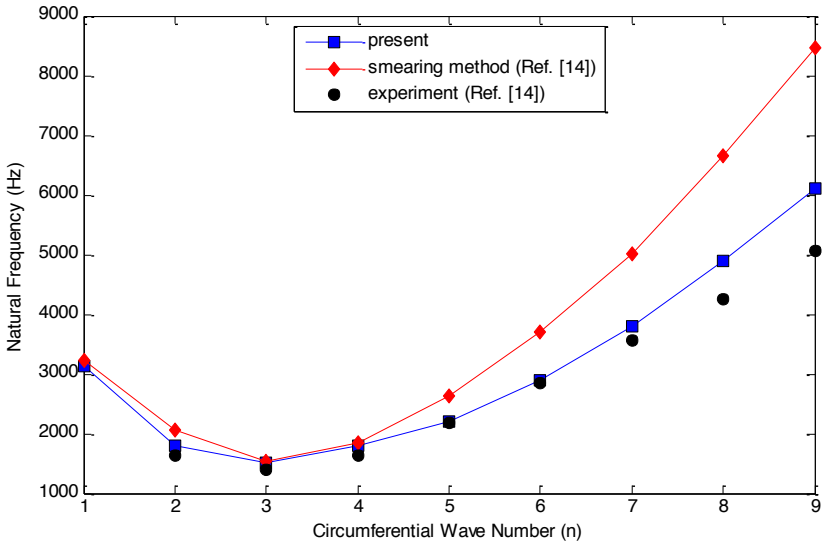

Figure 6 Variation of natural frequencies for the orthogonally stiffened isotropic conical shell with circumferential wave number in comparison between results of the present study and those reported in Ref. [14]. (L/a=3.06, h/a=0.0292, α=10°, m=1, Ω=0rev/s, N_s=6, N_r=3)

Fig. 7 (a-b) demonstrates that, for different boundary conditions considered here, variation of the frequency for unstiffened and stiffened conical shell decreases rapidly at first, and then raised monotonically by increasing the circumferential wave number, n. The Cs-Cl conical shell has the highest frequency, followed by the Ss-Cl , Cs-Sl and S-S shells. This behavior was simply expected before, as Cs-Cl is a fully restrained boundary condition. At lower circumferential wave numbers, relatively considerable differences between frequencies of the four boundary conditions are observed, implying that the influence of boundary condition is significant. At higher circum-

ferential wave numbers, the natural frequencies of Ss-Cl and Cs-Cl, and also those of Cs-Sl and Ss-Sl boundary conditions converge as a result of shortening the wavelengths. It should be noted that the effects of boundary condition are more significant for the unstiffened shell where the results of different boundary conditions are getting closer at mode number 8, though this occurred for the stiffened shell at mode number 6.

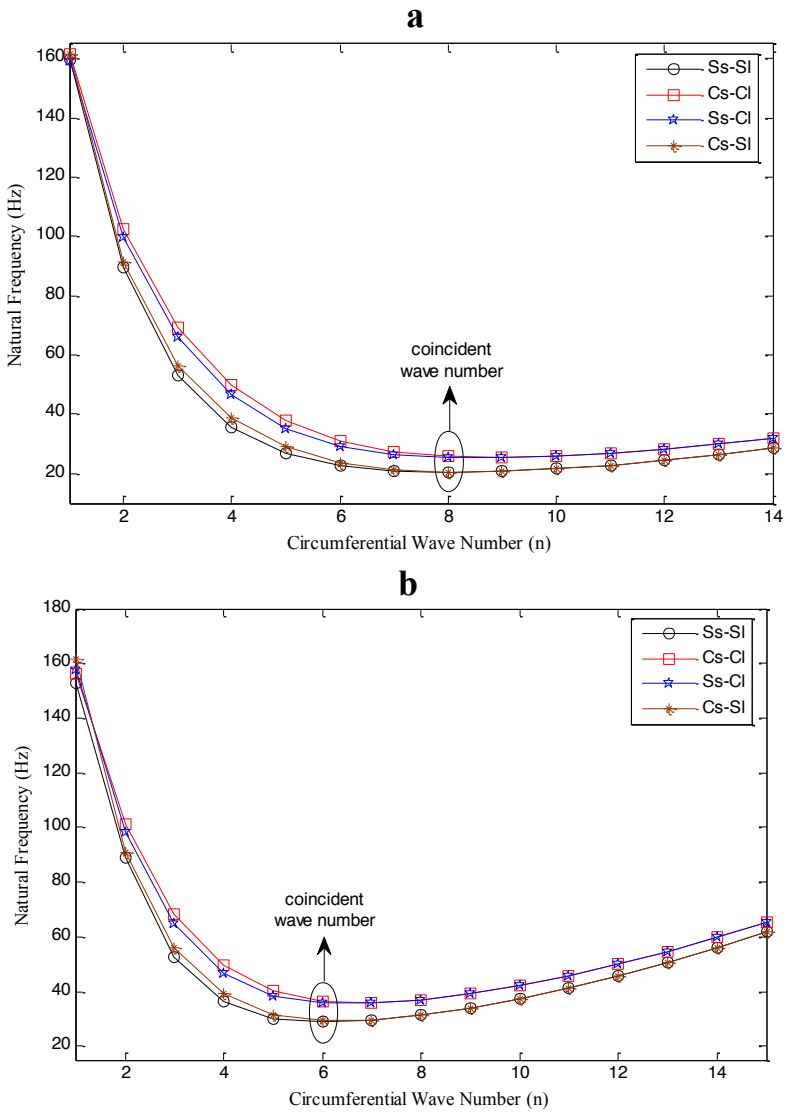

Figure 7 Variation of natural frequencies for the composite conical shell having circumferential wave number for different boundary conditions, (a) unstiffened shell, (b) stiffened shell $N_s=N_r=10$. (L=3m, a=0.5m, h=3mm, $\alpha=30^\circ$, m=1, $\Omega=0$, $[0^\circ/90^\circ/0^\circ]$)

Fig. 8 highlights the effects arisen from number of rings on frequencies of the stiffened non-rotating conical shell at fully clamped boundary conditions. No stringers are used in this case. It can be observed from this figure that at lower circumferential wave numbers, the number of rings demonstrates no significant effect. However, in high circumferential wave numbers, the frequency

is raised by increasing the number of rings, whereas the increasing rate of gradient becomes small. However, the number of circumferential waves with occurrence of the fundamental frequency decreases when the number of rings is enhanced. For example, the fundamental frequency occurred at $n=8$ for $N_r=0$, and at $n=5$ for $N_r=30$.

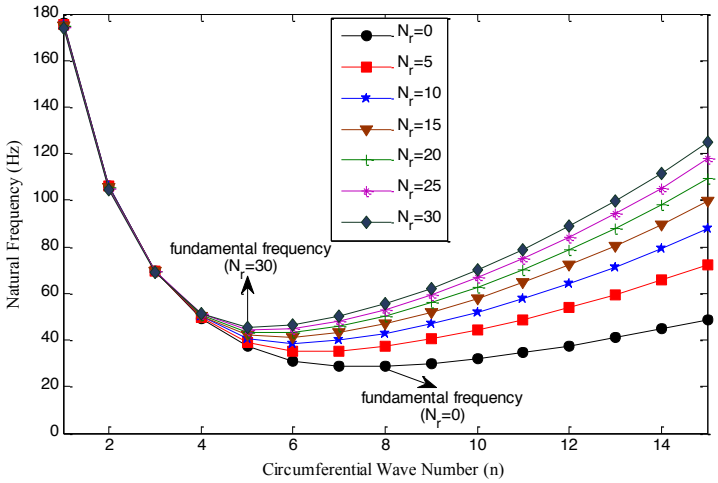

Figure 8 Variation of natural frequencies for the composite conical shell with circumferential wave number at various numbers of rings (L=3m, a=0.5m, h=3mm, α=20°, m=1, Ω=0, [0°/90°/0°], Cs-Cl)

Fig. 9 depicts the effects from number of stringers on natural frequency of the non-rotating stringer-stiffened conical shell. In this case, the numbers of stringers are 0, 10 and 20, where no rings are applied. It can be observed that the effect of stringers is negligible at great numbers of circumferential wave. However, at lower circumferential wave numbers, particularly in frequencies smaller than the fundamental one, the frequency decreases slightly by increasing the number of stringers. This is because inertial terms of the stiffened shell are more considerable than those of the stiffness.

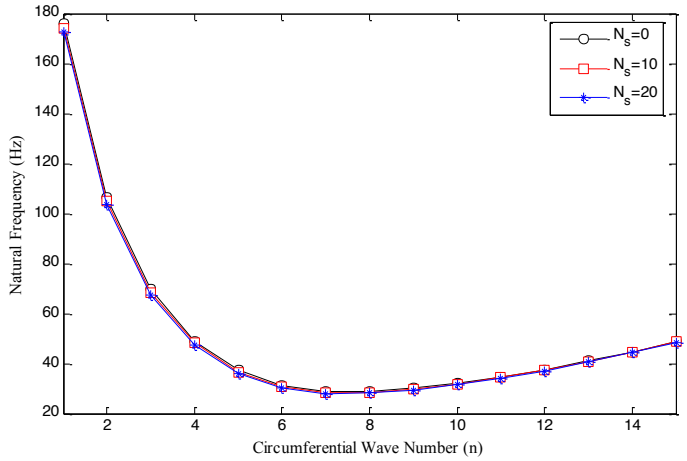

Figure 9 Variation of natural frequencies for the composite conical shell with circumferential wave number in various numbers of stringers (L=3m, a=0.5m, h=3mm, α=20°, m=1, Ω=0, [0°/90°/0°], Cs-Cl)

The effects of cone angles on natural frequency of the conical shells stiffened with rings and stringers at different circumferential wave numbers is listed in Tables 7 and 8, respectively. It is noteworthy that the number of rings in lower circumferential wave numbers, namely, n=2, are negligible for all cone angles. However, at greater number of circumferential wave the results are affected by the ring numbers. This occurrence is not the same in different cone angles. In smaller cone angles, the increasing rate is very significant. For instance, the natural frequencies are enhanced up to 304% in $\alpha=0^{o}$ when N_r is increased to 15. However, this effect is rather reduced for large cone angles; as in $\alpha=70^{o}$ the results are increased 108%. This is mainly due to the fact that flexural rigidity of the ring elements decreases at greater radius, while the terms of mass inertial increase. With greater number of the stringers a slight reduction is seen in natural frequency as listed in Table 8. This descending rate is more considerable at lower circumferential wave number and smaller cone angle. Therefore, the use of stringer is not recommended unless the buckling phenomenon is significant. The trend of results for natural frequency with respect to the cone angles in lower circumferential wave numbers contain a maximum point beyond which the trend will become descending.

Table 7 Variation of natural frequency for laminated conical shell with respect to number of rings and cone angles at various circumferential wave number (L=3m, a=0.5m, h=2mm, Ω=0, [0°/90°/0°], Ss-Sl)

		cone angle (α^{o})							
		0^{o}	**10^{o}**	**20^{o}**	**30^{o}**	**40^{o}**	**50^{o}**	**60^{o}**	**70^{o}**
	N_r								
n=2	0	53.2	73.6	85.8	89.9	86.3	75.4	59.1	39.9
	5	53.4	73.2	85.4	89.6	86.1	75.5	59.4	40.3
	10	53.6	72.8	84.9	89.2	85.9	75.5	59.6	40.6
	15	53.8	72.5	84.5	88.8	85.6	75.5	59.8	40.8
n=5	0	22.1	21.0	24.5	26.1	25.9	23.5	19.4	13.9
	5	53.9	30.7	28.3	28.1	27.0	24.5	20.3	15.0
	10	71.2	36.7	31.1	29.6	28.0	25.2	21.0	15.7
	15	83.6	41.1	33.2	30.8	28.8	25.8	21.6	16.3
n=10	0	81.4	31.4	21.1	17.6	15.3	13.2	10.9	8.5
	5	211.1	71.2	40.5	29.4	24.0	20.1	16.8	13.6
	10	279.9	90.0	51.0	35.5	28.3	23.6	19.6	16.0
	15	329.5	101.6	58.7	40.0	31.4	25.9	21.6	17.7

Table 8 Variation of natural frequency for laminated conical shell with respect to number of stringers and cone angles at various circumferential wave number (L=3m, a=0.5m, h=2mm, Ω=0, [0°/90°/0°], Ss-Sl)

		cone angle (α^o)							
	N_s	0^o	10^o	20^o	30^o	40^o	50^o	60^o	70^o
n=2	0	53.2	73.6	85.8	89.9	86.3	75.4	59.1	39.9
	5	50.7	71.8	84.6	89.2	85.8	75.1	58.8	39.7
	10	48.0	69.9	83.4	88.4	85.3	74.7	58.6	39.4
	15	45.3	68.0	82.1	87.6	84.8	74.4	58.3	39.1
n=5	0	22.1	21.0	24.5	26.1	25.9	23.5	19.4	13.9
	5	21.7	20.8	24.2	25.9	25.6	23.4	19.4	13.9
	10	21.4	20.5	24.0	25.8	25.5	23.3	19.3	13.9
	15	21.0	20.3	23.8	25.6	25.3	23.2	19.2	13.9
n=10	0	81.4	31.4	21.1	17.6	15.3	13.2	10.9	8.5
	5	80.4	31.2	21.0	17.5	15.3	13.1	10.9	8.5
	10	79.4	31.0	20.9	17.5	15.2	13.1	10.9	8.5
	15	78.5	30.8	20.8	17.4	15.1	13.0	10.8	8.5

Table 9 summarizes the effect of various shell lengths on natural frequency of the ring-stiffened shells with similar interval at different wave numbers. As mentioned above, natural frequencies are diminished by increasing the shell length as expected before. There is an exception for $a=0^o$, where for greater wave numbers, particularly $n=15$, increasing the shell length leads to enhanced corresponding natural frequencies. It is also noteworthy that fundamental wave numbers of the conical shell with $a=0^o$, 15^o are reduced monotonically with enlargement of the length. Although the trend is rather different at $a=45^o$, 60^o.

Table 9 Variation of natural frequency (Hz) for the laminated conical shell with respect to length of shells and cone angles in various circumferential wave number (a=1m, h=1mm, Ω=0, [0°/90°/0°], Cs-Cl)

L(m)	**2**			**5**			**8**		
α	**n=1**	**n=n_f***	**n=15**	**n=1**	**n=n_f**	**n=15**	**n=1**	**n=n_f**	**n=15**
0^o	247.8	50.7 (n=7)	145.9	102.5	23.1 (n=5)	157.3	59.4	14.9 (n=4)	160.1
15^o	227.5	44.6 (n=8)	84.0	104.7	19.0 (n=7)	43.6	67.2	12.2 (n=6)	25.2
30^o	188.4	38.9 (n=9)	58.7	94.9	16.1 (n=8)	23.2	63.2	9.8 (n=9)	12.7
45^o	134.6	32.8 (n=9)	45.2	71.5	13.2 (n=9)	16.2	48.4	7.8 (n=11)	8.7
60^o	84.4	26.0 (n=9)	35.9	44.5	10.1 (n=10)	12.1	30.1	5.8 (n=11)	6.4

Fig. 10(a-d) illustrates the effects of depth and width of ring cross-section on natural frequencies of backward waves for stiffened rotating conical shells having different cone angles. It is observed that at great circumferential wave numbers, frequencies of the shells generally increase with depth of the ring in both forward and backward waves. Moreover, the difference between curves becomes insignificant when the cone angle is raised. This is due to the fact that, inertia terms of the rings become more significant than the stiffening terms influenced by long depth of the rings where effective radius of the shell is increased.

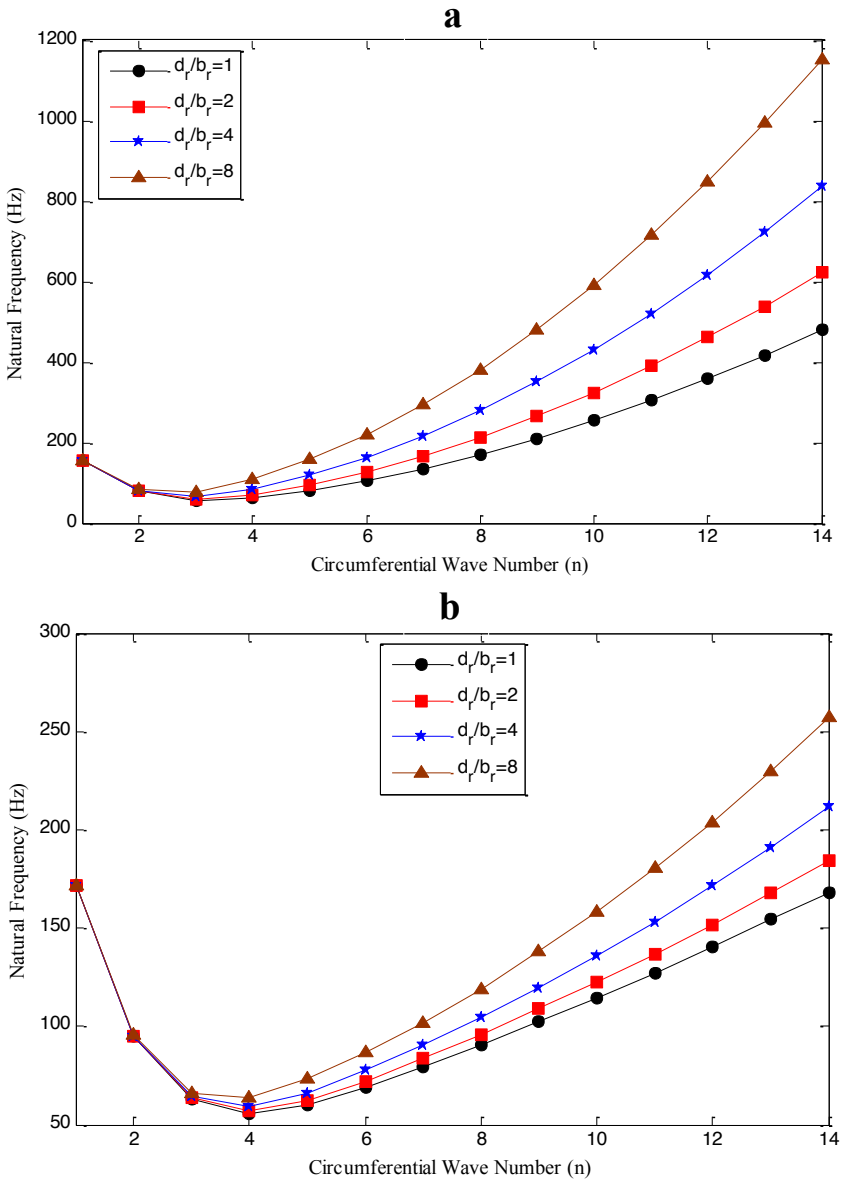

Figure 10 (continued) Variation of natural frequencies for the rotating ring-stiffened composite conical shell with circumferential wave number at various depth to width ratios, (a) $\alpha=0^{\circ}$, (b) $\alpha=15^{\circ}$, (c) $\alpha=30^{\circ}$, (d) $\alpha=45^{\circ}$. (L=3m, a=0.5m, h=3mm, m=1, $N_r=10$, $A_r=30mm^2$, $\Omega=10rev/sec$, $[0^{\circ}/90^{\circ}/0^{\circ}]$, Cs-Sl)

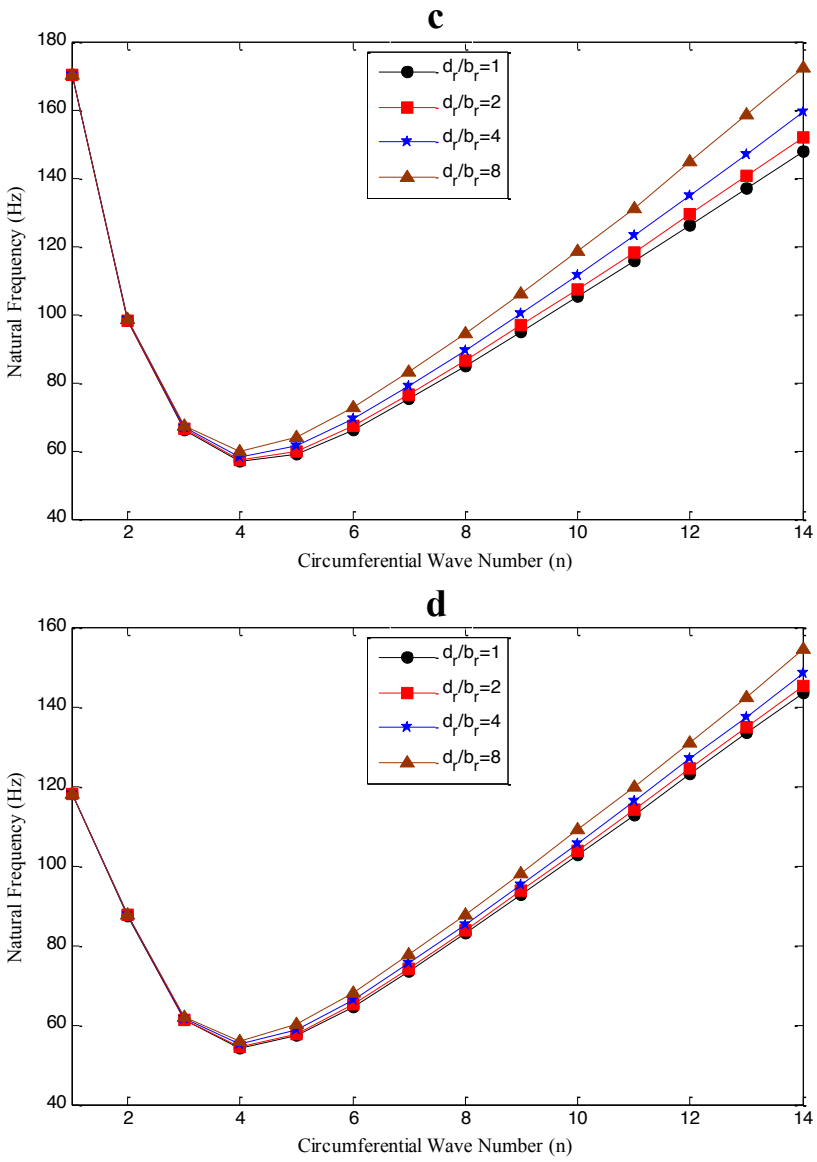

Figure 10 Variation of natural frequencies for the rotating ring-stiffened composite conical shell with circumferential wave number at various depth to width ratios, (a) $\alpha=0^{\circ}$, (b) $\alpha=15^{\circ}$, (c) $\alpha=30^{\circ}$, (d) $\alpha=45^{\circ}$. (L=3m, a=0.5m, h=3mm, m=1, $N_r=10$, $A_r=30mm^2$, $\Omega=10rev/sec$, $[0^{\circ}/90^{\circ}/0^{\circ}]$, Cs-Sl)

The phenomenon of critical speed of the shell is illustrated in Fig. 11. The critical speed of the rotating shell corresponds to rotational speed of the shell at which the forward wave intersects abscissa. At this inter-section, an unstable phenomenon possibly appears as the forward wave becomes standing with respect to the traveling coordinate and thus would be ready to switch to

backward mode. At this critical speed, any residual unbalance will be synchronized with the rotation and magnify whirling amplitude.

For various cone angles, α, the relationship between frequency and rotating speed at mode (1, 1) in the case of Ss-Sl boundary condition, is shown in Fig. 11. Contrary to cylindrical shell, variation of the natural frequency with rotating speed shows non-linearity in conical shell. This non-linearity is intensified with increased cone angle. Furthermore, critical speeds of the conical shell are enhanced due to greater cone angles, but there is no general rule to compare natural frequencies of the shells.

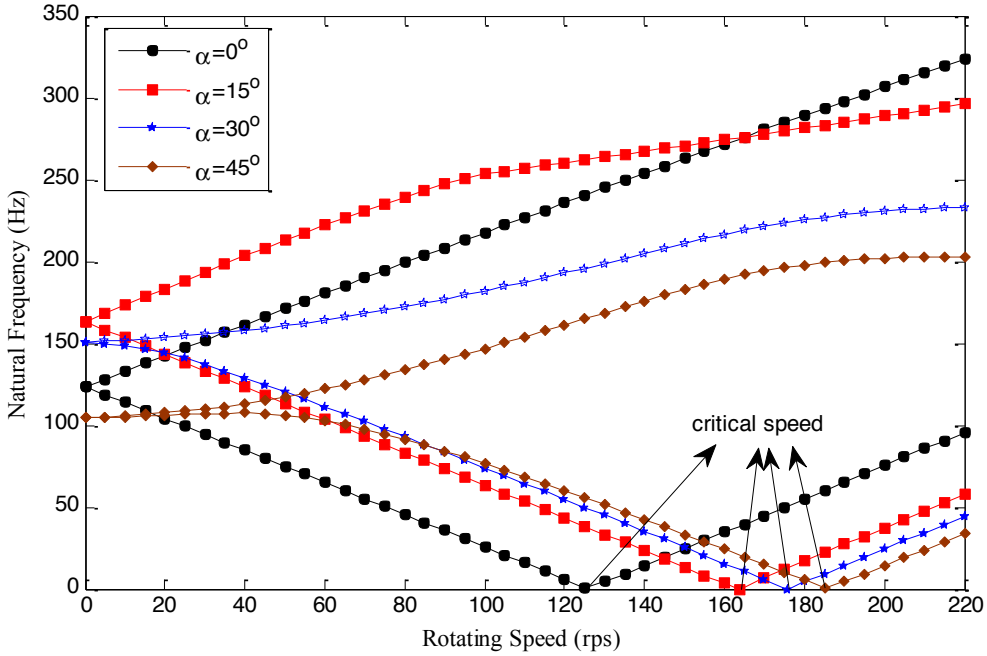

Figure 11 Variation of natural frequency of the rotating stiffened laminated conical shell with rotating speed at various cone angles (L=3m, a=0.5m, h=3mm, m=n=1, N_s=N_r=10, [0°/90°/0°], Ss-Sl)

Variations of natural frequency with rotating speed at different circumferential wave numbers are shown in Fig. 12(a-d) for various cone angles of the rotating stiffened conical shell with simply supported boundary conditions at both edges. The results in Fig. 12(a) indicate that critical speed of the cylindrical shell occurs in mode n=1, but, as can be seen in Fig. 12(b-d), the phenomenon of critical speed of the conical shell is observed for all circumferential wave numbers. Having compared the effects of rotating speed on the natural frequency, a significant difference between conical and cylindrical shells is noticed. It is noteworthy that the critical speed for *n=1* increases for greater values of the cone angle, contrary to all other circumferential wave numbers where the critical speeds decrease rapidly. For example, the critical speed of the conical shell at n=*1* is enhanced from 107(rev/sec) to 115(rev/sec) when the cone angles are altered from 30^o to 45^o. On the other hand, the critical speeds at n=2 are suddenly reduced from 359(rev/sec) to 270(rev/sec).

There is also another important discrepancy between rotating cylindrical and conical shells which is called divergence instability here. As seen from Fig. 12(a), the difference between fre-

quencies of backward and forward waves would increase when the rotating speed is raised. In the case of the conical shell, although the difference between frequencies of forward and backward waves increases initially, it decreases then. These two curves tend to overlap in a specific range of rotating speed. The divergence instability of the rotating shell corresponds to rotational speed of the shell where the frequencies of forward and backward waves are the same. The rotating speeds of divergence instability are generally higher than those of the critical one. This phenomenon is illustrated in Fig. 12(b-d). As can be clearly seen, raising the cone angle imposes a reduction in the rotating speed at which the divergence instability is occurred.

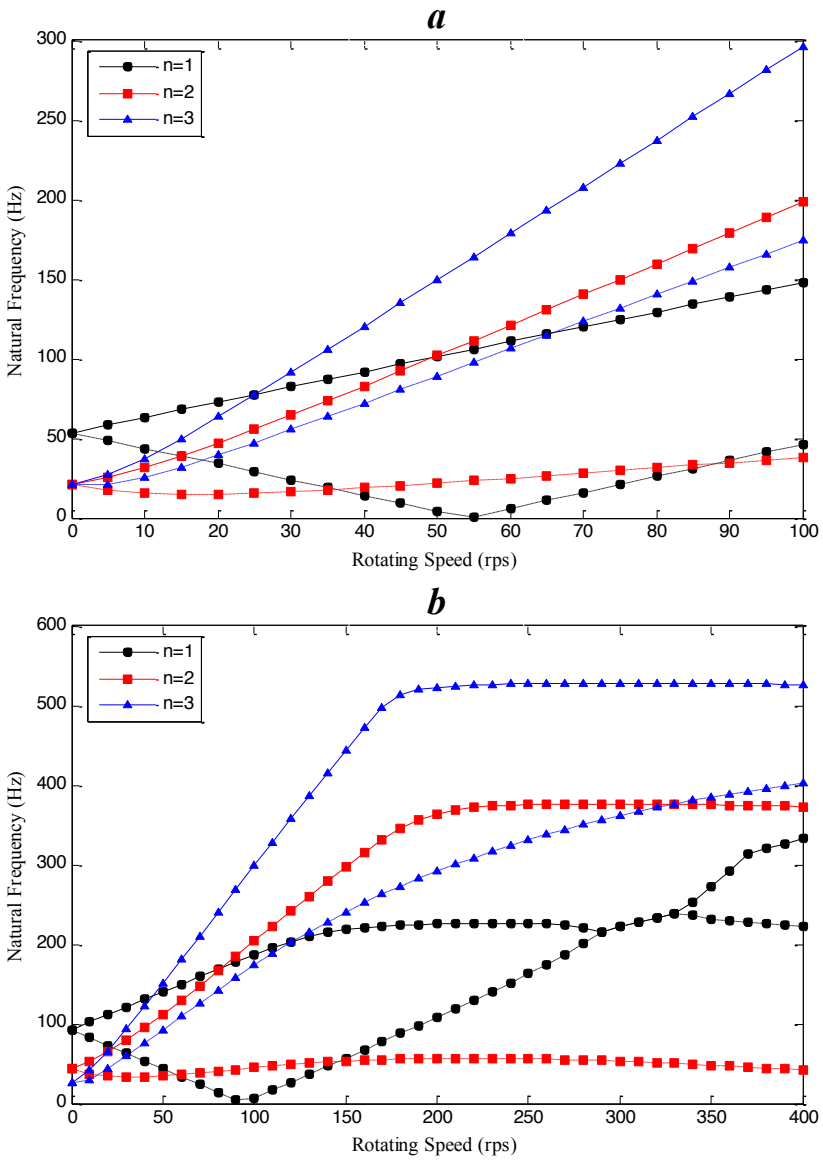

Figure 12 (continued) Variation of natural frequencies for the rotating stiffened composite conical shell with rotating speed at various cone angles, (a) α=0°, (b) α=15°, (c) α=30°, (d) α=45°. (L=5m, a=0.5m, h=3mm, m=n=1, N_s=N_r=10, [0°/90°/0°], Ss-Sl)

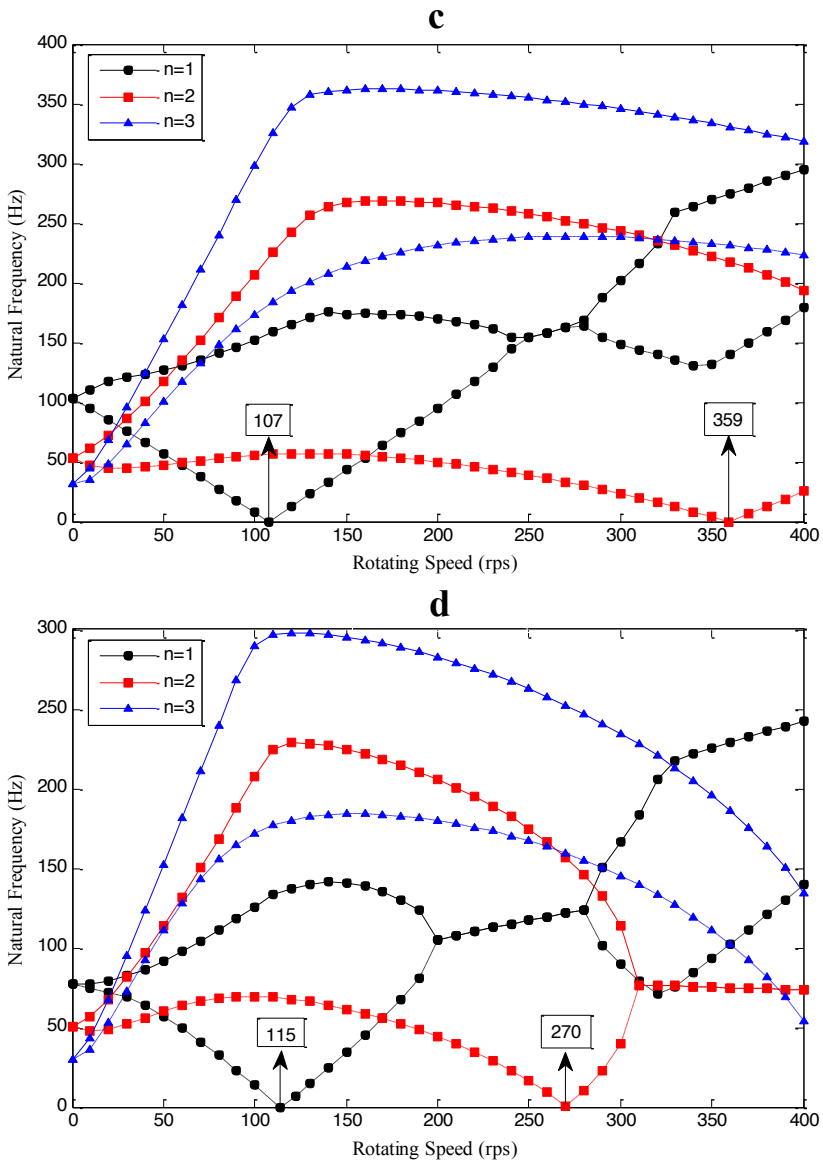

Figure 12 Variation of natural frequencies for the rotating stiffened composite conical shell with rotating speed at various cone angles, (a) α=0°, (b) α=15°, (c) α=30°, (d) α=45°. (L=5m, a=0.5m, h=3mm, m=n=1, N_s=N_r=10, [0°/90°/0°], Ss-Sl)

In Fig. 13(a-d), four configurations of the conical shell, namely at α=0°, 15°, 30° and 45°, are used to investigate the effect of axial load on natural frequency. In this figure, N_{cr}^{x} is used to address critical global buckling load of the conical shell, while axial compressive and tensile loads are represented by negative and positive signs, respectively. It is important to note that the compressive axial load must be a fraction of static critical global buckling load. To achieve the static critical global buckling load, the global buckling differential equations could be produced by ne-

glecting the terms involving Ω and ω in Eq. (52). The responses to both compressive and tensile axial loads are generally predictable for all modes having a downward and upward shift, respectively. This is expected since tensile axial load causes the shell to become stiffer. Noteworthy is that the effect of axial load on fundamental frequency is more significant than others. Moreover, the sensitivity rate of natural frequency to compressive load is greater than that of natural frequency to the tensile load.

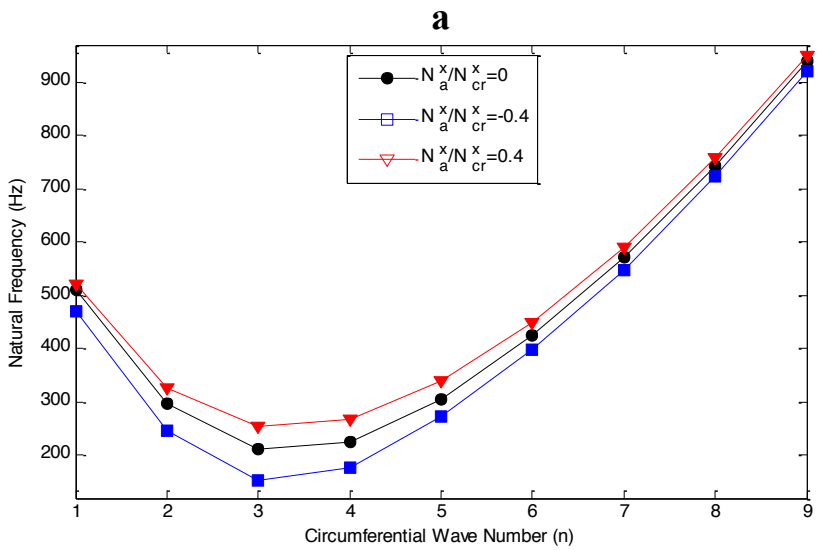

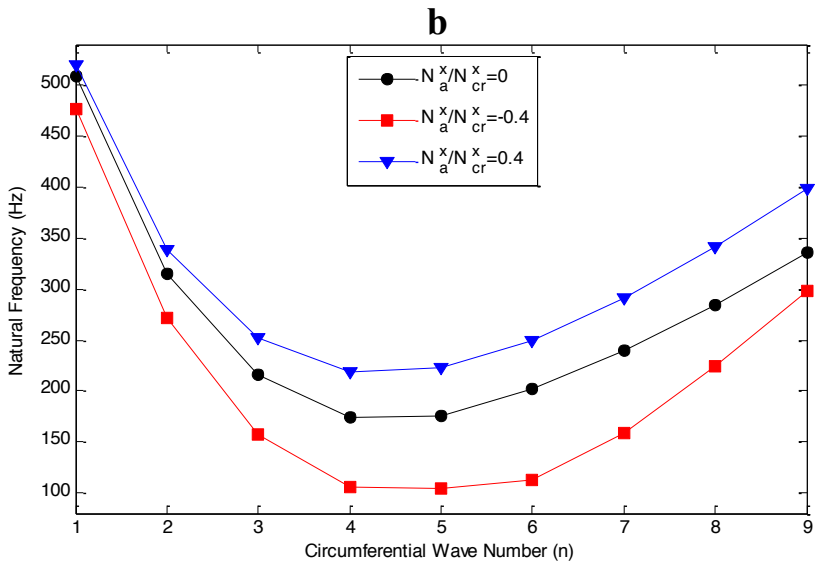

Figure 13 (continued) Variation of natural frequencies for the non-rotating stiffened composite conical shell with circumferential wave number at various cone angles, (a) α=0°, (b) α=15°, (c) α=30°, (d) α=45°. (L=1m, a=0.25m, h=3mm, m=1, N_s=N_r=5, [0°/90°/0°], Cs-Cl)

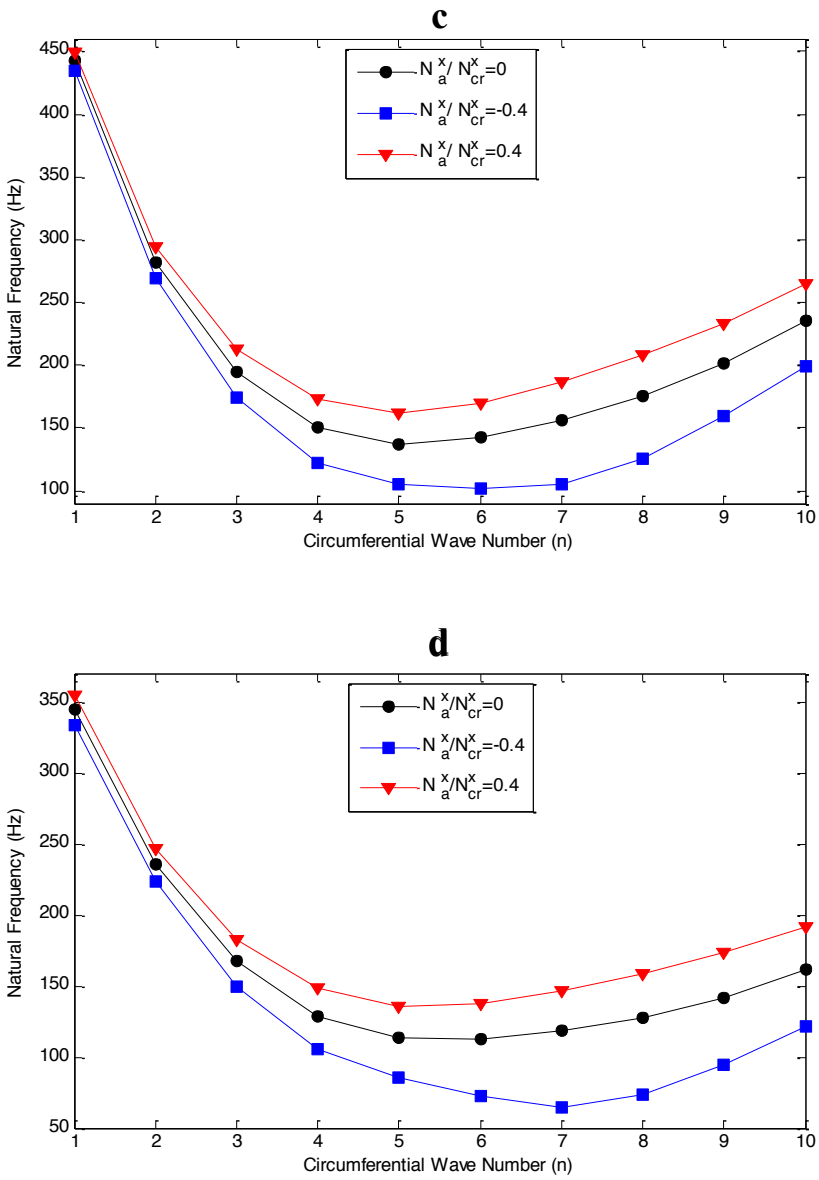

Figure 13 Variation of natural frequencies for the non-rotating stiffened composite conical shell with circumferential wave number at various cone angles, (a) α=0°, (b) α=15°, (c) α=30°, (d) α=45°. (L=1m, a=0.25m, h=3mm, m=1, N_s=N_r=5, [0°/90°/0°], Cs-Cl)

4. CONCLUSIONS

Generalized Differential Quadrature Method has been used in this paper to study free vibration and critical speed of the rotating stiffened laminated conical shells by treating the stiffeners as discrete elements. In addition, the FEM code was developed by the commercial FE software, ABAQUS. The results obtained from GDQM are validated in special cases with the results of present FE model and also those of other researchers. Discussions are made on the effects of boundary conditions, number of stiffeners, axial load, cone angle and rotating speed. Finally, the following results have been obtained:

1- The effect arisen from number of rings on natural frequency at lower circumferential wave numbers is negligible for all cone angles. However, in higher modes the results are affected by ring numbers with the variety of results having different cone angles being recognized. The natural frequencies are enhanced 304% at $\alpha=0^{o}$, while N_r is increased to 15. However, this rate will be reduced for high cone angles as in $\alpha=70^{o}$ the results are increased just 108%.

2- The trend of results for natural frequency with respect to cone angles at lower circumferential wave numbers contains a maximum point in which the trend for higher wave numbers becomes descending.

3- The present method is in agreement with the experiments. There is only an average of 10% discrepancy between the present work and those of experimental results for a widely stiffened conical shell from n=2 to n=9. However the inconsistency of 41% was reported by other researchers with the results of smearing method.

4- By increasing the number of stringers, a slight reduction is noticed in natural frequency. Therefore, application of stringer is not recommended unless the buckling phenomenon is significant.

5- The fundamental wave numbers of the conical shell with $\alpha=0^{o}$, 15^{o} are monotonically reduced with increasing the length, whereas a rather adverse trend is found at $\alpha=45^{o}$, 60^{o}.

6- Contrary to cylindrical shell, the variation of natural frequency with rotating speed behaves non-linearly in conical shell. In addition, the critical speed is recorded at all circumferential wave numbers. Moreover, the critical speeds of conical shell are enhanced due to increasing the cone angles.

7- Contrary to cylindrical shell, the phenomenon of divergence instability is occurred for rotating conical shell. Also, increasing the cone angle seems to impose reductions in rotating speed at which the divergence instability is occurred.

References

[1] Leissa, A.W.: *Vibration of shells*, NASA, SP-288 (1973)

[2] Soedel, W.: *Vibrations of shells and plates, Revised and expanded*, 2nd Ed., New York: Marcel Dekker (1996)

[3] Reddy, J.N.: *Mechanics of laminated composite plates and shells: theory and analysis*, 2nd Ed., CRC press (2004)

[4] Lam, K.Y., Loy, C.T.: On vibrations of thin rotating laminated composite cylindrical shells. *Composites Engineering* 4, 1153_1167 (1994)

[5] Lam, K.Y., Loy, C.T.: Free vibrations of a rotating multi-layered cylindrical shell. *Int J Solids Struct* 32, 647_663 (1995)

[6] Lam, K.Y., Loy, C.T.: Analysis of rotating laminated cylindrical shells by different thin shell theories. *J Sound Vibr* 186, 23_25 (1995)

[7] Hua, L., Lam, K.Y.: Frequency characteristics of a thin rotating cylindrical shell using the generalized differential quadrature method. *Int J Mech Sci* 40, 443_459 (1998)

[8] Chen, Y., Zhao, H.B., Shea, Z.P.: Vibrations of high speed rotating shells with calculations for cylindrical shells. *J Sound Vibr* 160, 137_160 (1993)

[9] Lindholm, U.S., Hu, W.C.L.: Non-symmetric transverse vibrations of truncated conical shells. *Intl J Mech Sci* 8 (9), 561_579 (1966)

[10] Lam, K.Y., Hua, L.: Vibration analysis of a rotating truncated circular conical shell. *Int J Solids Struct* 34 (17), 2183_2197 (1997)

[11] Lim, C.W., Liew, K.M.: Vibratory behaviour of shallow conical shells by a global Ritz formulation. *Eng Struct* 17(1), 63_70 (1995)

[12] Zhao, X., Liew, K.M., Ng, T.Y.: Vibration of rotating cross-ply laminated circular cylindrical shells with stringer and ring stiffeners. *Int J Solids Struct* 39, 529_545 (2002)

[13] Jafari, A.A., Bagheri, M.: Free vibration of rotating ring stiffened cylindrical shells with non-uniform stiffener distribution. *J Sound Vibr* 296, 353_376 (2006)

[14] Crenwelge, O.E., Muster, D.: Free vibration of ring and stringer stiffened conical shells. *J Acoust Soc Am* 46, 176_185 (1969)

[15] Rao, S.S., Reddy, E.S.: Optimum design of stiffened conical shells with natural frequency constraints. *Comput Struct* 14, 103_110 (1981)

[16] Langley, R.S.: A dynamic stiffness technique for the vibration analysis of stiffened shell structures. *J Sound Vibr* 156, 521_540 (1992)

[17] Raj, D.M., Narayanan, R., Khadakkar, A.G., Paramasivam, V.: Effect of ring stiffeners on vibration of cylindrical and conical shell models. *J Sound Vibr* 179, 413_426 (1995)

[18] Mecitoğlu, Z.: Vibration characteristics of a stiffened conical shell. *J Sound Vibr* 197 (2), 191_206 (1996)

[19] Goldfeld, Y.: Elastic buckling and imperfection sensitivity of generally stiffened conical shells. *AIAA Journal* 45 (3), 721_729 (2007)

[20] Jabareen, M., Sheinman, I.: Stability of imperfect stiffened conical shells. *Int J Solids Struct* 46 (10), 2111_2125 (2009)

[21] Farkas, J., Jármai, K., Orbán, F.: Cost minimization of a ring-stiffened conical shell loaded by external pressure. *Welding in the World* 52 (5-6), 110_115 (2008)

[22] Talebitooti, M., Ghayour, M., Ziaei-Rad, S., Talebitooti, R.: Free vibrations of rotating composite conical shells with stringer and ring stiffeners. *Arch Appl Mech* 80 (3), 201_215 (2010)

[23] Shu, C.: *Differential Quadrature and Its Application in Engineering*, Springer, Berlin (2000)

[24] Wang, Y., Liu, R., Wang, X.: On free vibration analysis of nonlinear piezoelectric circular shallow spherical shells by the differential quadrature element method. *J Sound Vib* 245, 179_185 (2001)

[25] Liew, K.M., Ng, T.Y., Zhang, J.Z.: Differential quadrature-layerwise modeling technique for three dimensional analysis of cross-ply laminated plates of various edge supports. *Comput Meth Appl Mech Eng* 191, 3811_3832 (2002)

[26] Karami, G., Malekzadeh, P.: A new differential quadrature methodology for beam analysis and the associated differential quadrature element method. *Comput Meth Appl Mech Eng* 191, 3509_3526 (2002)

[27] Ng, T.Y., Hua, L., Lam, K.Y.: Generalized differential quadrature for free vibration of rotating composite laminated conical shell with various boundary conditions. *Int J Mech Sci* 45, 567_587 (2003)

[28] Huang, Y.Q., Li, Q.S.: Bending and buckling analysis of antisymmetric laminates using the moving least square differential quadrature method. *Comput Meth Appl Mech Eng* 193, 3471_3492 (2004)

[29] Wang, X., Wang, Y.: Free vibration analyses of thin sector plates by the new version of differential quadrature method. *Comput Meth Appl Mech Eng* 193, 3957_3971 (2004)

[30] Wang, X.: Nonlinear stability analysis of thin doubly curved orthotropic shallow shells by the differential quadrature method. *Comput Meth Appl Mech Eng* 196, 2242_2251 (2007)

[31] Haftchenari, H., Darvizeh, M., Darvizeh, A., Ansari, R., Sharama, C.B.: Dynamic analysis of composite cylindrical shells using differential quadrature method(DQM). *Compos Struct* 78, 292_298 (2007)

[32] Nedelcu, M.: GBT formulation to analyse the buckling behaviour of isotropic conical shells. *Thin-Walled Struct* 49, 812-_818 (2011)

[33] Irie, T., Yamada, G., Tanaka, K.: Natural frequencies of truncated conical shells. *J Sound Vibr* 92, 447_453 (1984)

[34] Lam, K.Y., Hua, L.: Influence of boundary conditions on the frequency characteristics of a rotating truncated circular conical shell. *J Sound Vibr* 223 (2), 171_195 (1999)

Appendix A

$$M_{11} = \int_0^L \left(\pi\rho_{sh} h r_x + N_s \rho_s A_s\right) dx + \pi\rho_r A_r \sum_{k=1}^{N_r} \delta\left(x - x_k\right) r_x \tag{A1}$$

$$M_{13} = \frac{-N_s \rho_s A_s d_s}{2} \int_0^L \frac{\partial}{\partial x} dx - \frac{\pi\rho_r A_r d_r}{2} \sum_{k=1}^{N_r} \delta\left(x - x_k\right) \frac{\partial}{\partial x} r_x \tag{A2}$$

$$\begin{aligned} M_{22} &= \int_0^L \left[\pi\rho_{sh} h r_x + N_s \rho_s \left(A_s + \frac{I_S n^2}{r_x^2}\right)\right] dx \\ &+\pi\rho_r \left[A_r \sum_{k=1}^{N_r} \delta\left(x - x_k\right) r_x + I_r n^2 \sum_{k=1}^{N_r} \frac{\delta\left(x - x_k\right)}{r_x}\right] \end{aligned} \tag{A3}$$

$$M_{31} = \frac{N_s \rho_s A_s d_s}{2} \int_0^L \frac{\partial}{\partial x} dx + \frac{\pi\rho_r A_r d_r}{2} \sum_{k=1}^{N_r} \delta\left(x - x_k\right) \frac{\partial}{\partial x} r_x \tag{A4}$$

$$\begin{aligned} M_{33} &= \int_0^L \left[\pi\rho_{sh} h r_x + N_s \rho_s \left(A_s + \frac{I_S n^2}{r_x^2} - I_s \frac{\partial^2}{\partial x^2}\right)\right] dx \\ &+\pi\rho_r \left[A_r \sum_{k=1}^{N_r} \delta\left(x - x_k\right) r_{xk} + I_r n^2 \sum_{k=1}^{N_r} \frac{\delta\left(x - x_k\right)}{r_x} - I_r \sum_{k=1}^{N_r} \delta\left(x - x_k\right) r_x \frac{\partial^2}{\partial x^2}\right] \end{aligned} \tag{A5}$$

$$\begin{aligned} G_{12} &= \int_0^L \left(2\pi\rho_{sh} h \Omega r_x \sin\alpha + 2N_s \rho_s A_s \Omega \sin\alpha\right) dx \\ &+2\pi\rho_r A_r \Omega \sin\alpha \sum_{k=1}^{N_r} \delta\left(x - x_k\right) r_x \end{aligned} \tag{A6}$$

$$G_{13} = \int_0^L \frac{N_s \rho_s A_s d_s \Omega n \sin\alpha}{r_x} dx + \pi\rho_r A_r d_r \Omega n \sin\alpha \sum_{k=1}^{N_r} \delta\left(x - x_k\right) \tag{A7}$$

$$G_{21} = G_{12} \tag{A8}$$

$$G_{22} = \int_0^L \frac{-2N_s \rho_s A_s d_s \Omega n \cos\alpha}{r_x} dx - 2\pi\rho_r A_r d_r \Omega n \cos\alpha \sum_{k=1}^{N_r} \delta\left(x - x_k\right) \tag{A9}$$

$$G_{23}=\Omega\left\{\begin{array}{l}\int_0^L\left[2\pi\rho_{sh}hr_x\cos\alpha+N_s\rho_s\left(\begin{array}{l}2A_s\cos\alpha-A_sd_s\sin\alpha\dfrac{\partial}{\partial x}\\-\dfrac{2I_sn^2\cos\alpha}{r_x^2}\end{array}\right)\right]dx\\+\pi\rho_r\left[\begin{array}{l}2A_r\cos\alpha\sum_{k=1}^{N_r}\delta\left(x-x_k\right)r_x\\-A_rd_r\sin\alpha\sum_{k=1}^{N_r}\delta\left(x-x_k\right)r_x\dfrac{\partial}{\partial x}\\-2I_rn^2\cos\alpha\sum_{k=1}^{N_r}\dfrac{\delta\left(x-x_k\right)}{r_x}\end{array}\right]\end{array}\right\} \tag{A10}$$

$$G_{31}=G_{13} \tag{A11}$$

$$G_{32}=\Omega\left\{\begin{array}{l}\int_0^L\left[2\pi\rho_{sh}hr_x\cos\alpha+N_s\rho_s\left(\begin{array}{l}2A_s\cos\alpha+A_sd_s\sin\alpha\dfrac{\partial}{\partial x}\\-\dfrac{2I_sn^2\cos\alpha}{r_x^2}\end{array}\right)\right]dx\\+\pi\rho_r\left[\begin{array}{l}2A_r\cos\alpha\sum_{k=1}^{N_r}\delta\left(x-x_k\right)r_x\\+A_rd_r\sin\alpha\sum_{k=1}^{N_r}\delta\left(x-x_k\right)r_x\dfrac{\partial}{\partial x}\\-2I_rn^2\cos\alpha\sum_{k=1}^{N_r}\dfrac{\delta\left(x-x_k\right)}{r_x}\end{array}\right]\end{array}\right\} \tag{A12}$$

$$G_{33}=\int_0^L\frac{2N_s\rho_sA_sd_s\Omega n\cos\alpha}{r_x}dx+2\pi\rho_rA_rd_r\Omega n\cos\alpha\sum_{k=1}^{N_r}\delta\left(x-x_k\right) \tag{A13}$$

$$\begin{array}{l}K_{11}=\int_0^L\left\{\begin{array}{l}\pi r_x\left(\rho_{sh}h\Omega^2\sin^2\alpha+A_{11}\dfrac{\partial^2}{\partial x^2}-\dfrac{A_{22}\sin^2\alpha+A_{66}n^2}{r_x^2}\right)\\+N_sA_s\left(E_s\dfrac{\partial^2}{\partial x^2}+\rho_s\Omega^2\sin\alpha\right)\end{array}\right\}dx\\-\pi E_rA_r\sin^2\alpha\sum_{k=1}^{N_r}\dfrac{\delta\left(x-x_k\right)}{r_x}+\pi\rho_rA_r\Omega^2\sin\alpha\sum_{k=1}^{N_r}\delta\left(x-x_k\right)r_x\end{array} \tag{A14}$$

$$K_{12}=\int_0^L\left\{\begin{array}{l}-\pi r_x\left[\dfrac{\left(A_{22}+A_{66}\right)n\sin\alpha}{r_x^2}-\dfrac{\left(A_{66}+A_{12}\right)n}{r_x}\dfrac{\partial}{\partial x}\right]\\-\dfrac{N_sA_sd_s\rho_sn\Omega^2\sin\alpha\cos\alpha}{2r_x}\end{array}\right\}dx$$
$$-\pi E_rA_r\left[n\sin\alpha\sum_{k=1}^{N_r}\frac{\delta\left(x-x_k\right)}{r_x}-d_rn\cos\alpha\sin\alpha\sum_{k=1}^{N_r}\frac{\delta\left(x-x_k\right)}{2r_x^2}\right] \tag{A15}$$
$$-\frac{\pi\rho_rA_rd_rn\Omega^2\sin\alpha\cos\alpha}{2}\sum_{k=1}^{N_r}\delta\left(x-x_k\right)$$

$$K_{13}=\int_0^L\left\{\begin{array}{l}\pi r_x\left(\rho_{sh}h\Omega^2\sin\alpha\cos\alpha+\dfrac{A_{12}\cos\alpha}{r_x}\dfrac{\partial}{\partial x}-\dfrac{A_{22}\sin\alpha\cos\alpha}{r_x^2}\right)\\+N_sA_s\left(-\dfrac{E_sd_s}{2}\dfrac{\partial^3}{\partial x^3}+\rho_s\Omega^2\sin\alpha\cos\alpha-\dfrac{\rho_sd_s\Omega^2\sin^2\alpha}{2}\dfrac{\partial}{\partial x}\right)\end{array}\right\}dx$$
$$-\pi E_rA_r\left(\begin{array}{l}d_rn^2\sin\alpha\displaystyle\sum_{k=1}^{N_r}\frac{\delta\left(x-x_k\right)}{2r_x^2}-d_r\sin^2\alpha\sum_{k=1}^{N_r}\frac{\delta\left(x-x_k\right)}{2r_x}\frac{\partial}{\partial x}\\+\sin\alpha\cos\alpha\displaystyle\sum_{k=1}^{N_r}\frac{\delta\left(x-x_k\right)}{r_x}\end{array}\right) \tag{A16}$$
$$+\pi\rho_rA_r\left(\begin{array}{l}\Omega^2\sin\alpha\cos\alpha\displaystyle\sum_{k=1}^{N_r}\delta\left(x-x_k\right)r_x\\-d_r\Omega^2\sin^2\alpha\displaystyle\sum_{k=1}^{N_r}\frac{\delta\left(x-x_k\right)}{2}r_x\frac{\partial}{\partial x}\end{array}\right)$$

$$K_{21}=\int_0^L\left\{\begin{array}{l}-\pi r_x\left[\dfrac{\left(A_{22}+A_{66}\right)n\sin\alpha}{r_x^2}+\dfrac{\left(A_{66}+A_{12}\right)n}{r_x}\dfrac{\partial}{\partial x}\right]\\-\dfrac{N_sA_sd_s\rho_sn\Omega^2\sin\alpha\cos\alpha}{2r_x}\end{array}\right\}dx$$
$$-\pi E_rA_r\left[n\sin\alpha\sum_{k=1}^{N_r}\frac{\delta\left(x-x_k\right)}{r_x}-d_rn\cos\alpha\sin\alpha\sum_{k=1}^{N_r}\frac{\delta\left(x-x_k\right)}{2r_x^2}\right] \tag{A17}$$
$$-\frac{\pi\rho_rA_rd_rn\Omega^2\sin\alpha\cos\alpha}{2}\sum_{k=1}^{N_r}\delta\left(x-x_k\right)$$

$$
\begin{aligned}
K_{22} = \int_0^L \left\{ \begin{array}{l}
\pi r_x \left[\begin{array}{l}
\rho_{sh} h \Omega^2 - \dfrac{A_{22} n^2 + A_{66} \sin^2 \alpha}{r_x^2} \\
- \dfrac{D_{22} n^2 \cos^2 \alpha + 4 D_{66} \sin^2 \alpha \cos^2 \alpha}{r_x^4} \\
+ \left(A_{66} + \dfrac{4 D_{66} \cos^2 \alpha}{r_x^2} \right) \dfrac{\partial^2}{\partial x^2} - \rho_{sh} h \Omega^2 \left(\cos^2 \alpha + n^2 \right)
\end{array} \right] \\
+ N_s \left[\begin{array}{l}
G_s J_s \left(\dfrac{\cos^2 \alpha}{r_x^2} \dfrac{\partial^2}{\partial x^2} - \dfrac{4 \sin^2 \alpha \cos^2 \alpha}{r_x^4} \right) \\
+ \rho_s A_s \Omega^2 + \rho_s I_s n^2 \Omega^2 \cos^2 \alpha
\end{array} \right]
\end{array} \right\} dx \\
- \pi E_r \left[\begin{array}{l}
A_r n^2 \sum_{k=1}^{N_r} \dfrac{\delta\left(x - x_k \right)}{r_x} + I_r n^2 \cos^2 \alpha \sum_{k=1}^{N_r} \dfrac{\delta\left(x - x_k \right)}{r_x^3} \\
- A_r d_r n^2 \cos \alpha \sum_{k=1}^{N_r} \dfrac{\delta\left(x - x_k \right)}{r_x^2}
\end{array} \right] \\
+ \pi \rho_r \left[\begin{array}{l}
A_r \Omega^2 \left(1 - n^2 - \cos^2 \alpha \right) \sum_{k=1}^{N_r} \delta\left(x - x_k \right) r_x \\
+ I_r \Omega^2 \left(n^2 \cos^2 \alpha \sum_{k=1}^{N_r} \delta\left(x - x_k \right) - \left(n^4 + n^2 \cos^2 \alpha \right) \sum_{k=1}^{N_r} \dfrac{\delta\left(x - x_k \right)}{r_x} \right) \\
- 2 n^2 \Omega^2 A_r d_r \cos \alpha \sum_{k=1}^{N_r} \delta\left(x - x_k \right)
\end{array} \right]
\end{aligned}
\tag{A18}
$$

$$
\begin{aligned}
K_{23} = \int_0^L \Bigg\{ & \pi r_x \left(\begin{array}{l} \dfrac{-A_{22} n}{r_x^2} - \dfrac{D_{22} n^3 + 4 D_{66} n \sin^2\alpha}{r_x^4} \\ + \dfrac{D_{22} n \sin\alpha}{r_x^3} \dfrac{\partial}{\partial x} + \left(\dfrac{4D_{66} + D_{12}}{r_x^2} \right) n \dfrac{\partial^2}{\partial x^2} \\ -\rho_{sh} h \Omega^2 \left(2n \right) \end{array} \right) \cos\alpha \\
& + N_s \left(\begin{array}{l} \dfrac{G_s J_s n \cos\alpha}{r_x^2} \dfrac{\partial^2}{\partial x^2} - \dfrac{4 \sin^2\alpha \cos\alpha}{r_x^4} \\ + \dfrac{\rho_s n \Omega^2 \left(A_s d_s \sin^2\alpha + 2 I_s \cos\alpha \sin\alpha \dfrac{\partial}{\partial x} \right)}{2 r_x} \end{array} \right) \Bigg\} dx \\
& - \pi E_r A_r \left[\begin{array}{l} n \cos\alpha \displaystyle\sum_{k=1}^{N_r} \frac{\delta\left(x - x_k \right)}{r_x} + d_r n^3 \sum_{k=1}^{N_r} \frac{\delta\left(x - x_k \right)}{2 r_x^2} \\ - d_r n \sin\alpha \displaystyle\sum_{k=1}^{N_r} \frac{\delta\left(x - x_k \right)}{2 r_x} \frac{\partial}{\partial x} - d_r n \cos^2\alpha \sum_{k=1}^{N_r} \frac{\delta\left(x - x_k \right)}{2 r_x^2} \end{array} \right] \\
& + \pi E_r I_r \left[n^3 \cos\alpha \sum_{k=1}^{N_r} \frac{\delta\left(x - x_k \right)}{r_x^3} - n \cos\alpha \sin\alpha \sum_{k=1}^{N_r} \frac{\delta\left(x - x_k \right)}{r_x^2} \frac{\partial}{\partial x} \right] \\
& + \pi \rho_r \Omega^2 \left[\begin{array}{l} \dfrac{A_r n \left(d_r \sin^2\alpha - 4\cos\alpha \right)}{2} \displaystyle\sum_{k=1}^{N_r} \delta\left(x - x_k \right) \\ + I_r n \cos\alpha \sin\alpha \displaystyle\sum_{k=1}^{N_r} \delta\left(x - x_k \right) \frac{\partial}{\partial x} \\ + 2 I_r n^3 \cos\alpha \displaystyle\sum_{k=1}^{N_r} \frac{\delta\left(x - x_k \right)}{r_x} \end{array} \right]
\end{aligned}
\tag{A19}
$$

$$
\begin{aligned}
K_{31} = \int_0^L \Bigg\{ & \pi r_x \left(\rho_{sh} h \Omega^2 \sin\alpha \cos\alpha - \frac{A_{12} \cos\alpha}{r_x} \frac{\partial}{\partial x} - \frac{A_{22} \sin\alpha \cos\alpha}{r_x^2} \right) \\
& + N_s A_s \left(\frac{E_s d_s}{2} \frac{\partial^3}{\partial x^3} + \rho_s \Omega^2 \sin\alpha \cos\alpha + \frac{\rho_s d_s \Omega^2 \sin^2\alpha}{2} \frac{\partial}{\partial x} \right) \Bigg\} dx \\
& - \pi E_r A_r \left(\begin{array}{l} d_r n^2 \sin\alpha \displaystyle\sum_{k=1}^{N_r} \frac{\delta\left(x - x_k \right)}{2 r_x^2} + d_r \sin^2\alpha \sum_{k=1}^{N_r} \frac{\delta\left(x - x_k \right)}{2 r_x} \frac{\partial}{\partial x} \\ + \sin\alpha \cos\alpha \displaystyle\sum_{k=1}^{N_r} \frac{\delta\left(x - x_k \right)}{r_x} \end{array} \right) \\
& + \pi \rho_r A_r \left(\begin{array}{l} \Omega^2 \sin\alpha \cos\alpha \displaystyle\sum_{k=1}^{N_r} \delta\left(x - x_k \right) r_x \\ + d_r \Omega^2 \sin^2\alpha \displaystyle\sum_{k=1}^{N_r} \frac{\delta\left(x - x_k \right)}{2} r_x \frac{\partial}{\partial x} \end{array} \right)
\end{aligned}
\tag{A20}
$$

$$
\begin{aligned}
K_{32} = \int_0^L \left\{ \begin{array}{l}
\pi r_x \left(\begin{array}{l}
\dfrac{-A_{22} n}{r_x^2} - \dfrac{D_{22} n^3 + 4 D_{66} n \sin^2\alpha}{r_x^4} \\
- \dfrac{D_{22} n \sin\alpha}{r_x^3} \dfrac{\partial}{\partial x} + \left(\dfrac{4D_{66} + D_{12}}{r_x^2} \right) n \dfrac{\partial^2}{\partial x^2} \\
- \rho_{sh} h \Omega^2 \left(2n \right)
\end{array} \right) \cos\alpha \\
+ N_s \left(\begin{array}{l}
\dfrac{G_s J_s n \cos\alpha}{r_x^2} \dfrac{\partial^2}{\partial x^2} - \dfrac{4 \sin^2\alpha \cos\alpha}{r_x^4} \\
+ \dfrac{\rho_s n \Omega^2 \left(A_s d_s \sin^2\alpha - 2 I_s \cos\alpha \sin\alpha \dfrac{\partial}{\partial x} \right)}{2 r_x}
\end{array} \right)
\end{array} \right\} dx \\
- \pi E_r A_r \left[\begin{array}{l}
n \cos\alpha \sum_{k=1}^{N_r} \dfrac{\delta\left(x - x_k \right)}{r_x} + d_r n^3 \sum_{k=1}^{N_r} \dfrac{\delta\left(x - x_k \right)}{2 r_x^2} \\
- d_r n \sin\alpha \sum_{k=1}^{N_r} \dfrac{\delta\left(x - x_k \right)}{2 r_x} \dfrac{\partial}{\partial x} - d_r n \cos^2\alpha \sum_{k=1}^{N_r} \dfrac{\delta\left(x - x_k \right)}{2 r_x^2}
\end{array} \right] \\
+ \pi E_r I_r \left[n^3 \cos\alpha \sum_{k=1}^{N_r} \dfrac{\delta\left(x - x_k \right)}{r_x^3} + n \cos\alpha \sin\alpha \sum_{k=1}^{N_r} \dfrac{\delta\left(x - x_k \right)}{r_x^2} \dfrac{\partial}{\partial x} \right] \\
+ \pi \rho_r \Omega^2 \left[\begin{array}{l}
\dfrac{A_r n \left(d_r \sin^2\alpha - 4 \cos\alpha \right)}{2} \sum_{k=1}^{N_r} \delta\left(x - x_k \right) \\
- I_r n \cos\alpha \sin\alpha \sum_{k=1}^{N_r} \delta\left(x - x_k \right) \dfrac{\partial}{\partial x} \\
+ 2 I_r n^3 \cos\alpha \sum_{k=1}^{N_r} \dfrac{\delta\left(x - x_k \right)}{r_x}
\end{array} \right]
\end{aligned}
\tag{A21}
$$

$$
\begin{aligned}
K_{33} = \int_0^L \Bigg\{ & \pi r_x \left[\begin{array}{l} \rho_{sh} h \Omega^2 \cos^2\alpha - \dfrac{A_{22}\cos^2\alpha}{r_x^2} \\ -\dfrac{D_{22} n^4 + 4 D_{66} n^2 \sin^2\alpha}{r_x^4} \\ +\left(\dfrac{D_{22}\sin^2\alpha + \left(4D_{66} + 2D_{12}\right) n^2}{r_x^2} \right) \dfrac{\partial^2}{\partial x^2} \\ -D_{11}\dfrac{\partial^2}{\partial x^4} - \rho_{sh} h \Omega^2 \left(\cos^2\alpha + n^2 \right) \end{array} \right] \\
& + N_s \left[\begin{array}{l} -E_s I_s \dfrac{\partial^4}{\partial x^4} + G_s J_s \left(\dfrac{n^2}{r_x^2}\dfrac{\partial^2}{\partial x^2} - \dfrac{4\sin^2\alpha n^2}{r_x^4} \right) \\ +\rho_s A_s \Omega^2 \cos^2\alpha + \dfrac{\rho_s I_s n^2 \Omega^2}{r_x^2} \\ -\rho_s I_s \Omega^2 \sin^2\alpha \dfrac{\partial^2}{\partial x^2} \end{array} \right] \Bigg\} dx \\
& - \pi E_r \left[\begin{array}{l} A_r \cos^2\alpha \sum_{k=1}^{N_r} \dfrac{\delta\left(x - x_k\right)}{r_x} + I_r n^4 \sum_{k=1}^{N_r} \dfrac{\delta\left(x - x_k\right)}{r_x^3} \\ +A_r d_r n^2 \cos\alpha \sum_{k=1}^{N_r} \dfrac{\delta\left(x - x_k\right)}{r_x^2} - I_r \sin^2\alpha \sum_{k=1}^{N_r} \dfrac{\delta\left(x - x_k\right)}{r_x} \dfrac{\partial^2}{\partial x^2} \end{array} \right] \\
& + \pi G_r J_r n^2 \sum_{k=1}^{N_r} \dfrac{\delta\left(x - x_k\right)}{r_x} \dfrac{\partial^2}{\partial x^2} \\
& + \pi \rho_r \left[\begin{array}{l} -A_r \Omega^2 n^2 \sum_{k=1}^{N_r} \delta\left(x - x_k\right) r_x \\ +I_r \Omega^2 \left(\begin{array}{l} \left(n^2 \sin^2\alpha - n^4\right) \sum_{k=1}^{N_r} \dfrac{\delta\left(x - x_k\right)}{r_x} \\ -\sin^2\alpha \sum_{k=1}^{N_r} \delta\left(x - x_k\right) r_x \dfrac{\partial^2}{\partial x^2} \end{array} \right) \\ -2 A_r d_r n^2 \Omega^2 \cos\alpha \sum_{k=1}^{N_r} \delta\left(x - x_k\right) \end{array} \right]
\end{aligned}
\tag{A22}
$$

$$
M_{12} = M_{21} = M_{23} = M_{32} = G_{11} = 0 \tag{A23}
$$

where $\lambda = \dfrac{m\pi}{L}$.